Imaging the Growth of Recent Faults: The Case of 2016-2017 Seismic Sequence Sea Bottom Deformation in the Alboran Sea (Western Mediterranean)

J. Galindo-zaldivar, G. Ercilla, F. Estrada, M. Catalán, Elia d'Acremont, O. Azzouz, D. Casas, M. Chourak, J. T. Vazquez, A. Chalouan, et al.

Imaging the growth of recent faults: the case of 2016-17 seismic sequence sea bottom deformation in the Alboran Sea (Western Mediterranean)

J. Galindo-Zaldivar[1,2,*], G. Ercilla[3], F. Estrada[3], M. Catalán[4], E. d'Acremont[5], O. Azzouz[6], D. Casas[7], M. Chourak[6], J. T. Vazquez[8], A. Chalouan[9], C. Sanz de Galdeano[1], M. Benmakhlouf[10], C. Gorini[5], B. Alonso[3], D. Palomino[8], J. A. Rengel[11], A. J. Gil[12,13]

[1]Instituto Andaluz de Ciencias de la Tierra, CSIC- UGR, Granada 18071, Spain.

[2]Dpto. de Geodinámica, Universidad de Granada, Granada 18071, Spain.

[3]Institut de Ciències del Mar, GMC, ICM-CSIC, Barcelona 08003, Spain.

[4]Real Instituto y Observatorio de la Armada, San Fernando 11100 Cádiz, Spain.

[5]Sorbonne Universités, UPMC Université Paris 06, UMR 7193, ISTeP, F-75005, Paris, France.

[6]Université Mohammed Premier, Oujda, Morocco.

[7]Instituto Geológico y Minero de España, Granada, Spain.

[8]Instituto Español de Oceanografía, 29640, Fuengirola, Spain.

[9]Faculté des Sciences, Université Mohammed V-Agdal, Rabat, Morocco.

[10]Faculté des Sciences, Université Abdelmalek Essaadi, Tetouan, Morocco.

[11]Instituto Hidrográfico de la Marina IHM, Cádiz, Spain.

[12]Dpto. Ing. Cartográfica, Geodesia y Fotogrametría, Universidad de Jaén, 23071 Jaén, Spain.

[13]CEACTierra, Universidad de Jaén, 23071 Jaén, Spain.

Contact details:

Jesús Galindo-Zaldívar

Telephone: +34 958 243349

Fax: +34 958 248527

Email: jgalindo@ugr.es

Key Points:

The 2016-17 seismic sequence is related to the wide NNE-SSW sinistral fault zone located in the central part of the Alboran Sea.

Epicentral seabottom deformations include mass transport deposits and recent faults.

Seismicity and seabottom deformations are located west of the main Al Idrisi Fault, supporting the westward widening of the fault zone.

Abstract

The Eurasian-African NW-SE oblique plate convergence produces shortening and orthogonal extension in the Alboran Sea Basin (Westernmost Mediterranean), located between the Betic and Rif cordilleras. A NNE-SSW broad band of deformation and seismicity affects the Alboran central part. After the 1993-94 and 2004 seismic series, an earthquake sequence struck mainly its southern sector in 2016-17 (main event Mw=6.3, Jan 25, 2016). The near-surface deformation is investigated using seismic profiles, multibeam bathymetry, gravity and seismicity data. Epicentres can be grouped into two main alignments. The northern WSW-ENE alignment has reverse earthquake focal mechanisms and in its epicentral region recent mass-transport deposits occur. The southern alignment consists of a NNE-SSW vertical sinistral deformation zone, with early epicentres of higher magnitude earthquakes located along a narrow band 5 to 10 km offset westward of the Al Idrisi Fault. Here, near-surface deformation includes active NW-SE vertical and normal faults, unmapped until now. Later epicentres spread eastward, reaching the Al Idrisi Fault, characterized by discontinuous active NNE-SSW vertical fractures. Seismicity and tectonic structures suggest a westward propagation of deformation and the growth at depth of incipient faults, comprising a NNE-SSW sinistral fault zone in depth that is connected upwards with NW-SE vertical and normal faults. This recent fault zone is segmented and responsible for the seismicity in 1993-94 in the coastal area, in 2004 onshore and in 2016-17 offshore. Insights for seismic hazard assessment point to the growth of recent faults that could produce potentially higher magnitude earthquakes than the already formed faults.

Key words: Eurasian-African plate boundary; fault development; seismicity; mass transport deposits; active sea bottom deformations.

1. Introduction

Continuous plate motion has led to the activity of tectonic structures developed along plate boundaries, including faults with related seismicity. Seismic or creep behaviour of a fault is constrained by the rheology of the deformed rocks (Sibson, 1977). Brittle deformation is generally accommodated by previous fractures because the low cohesion with respect to the undeformed host rock causes them to be more easily reactivated (Anderson, 1951; Bott, 1959). When deformation propagates, the growth of fault zones is produced by stress concentrations at the boundaries of previous fault surfaces (Scholz, 1989) and the larger the fault, the higher the magnitude of the related earthquakes (Wells & Coppersmith, 1994). The activity of a fault requires the shear stress on its surface to exceed the values of cohesion and friction (Hajiabdolmajid et al., 2002). On a fault surface, the cohesion is low and needs lower shear stresses than on the new developing fault segments at the edge of the previous fault (Hajiabdolmajid et al., 2002). Thus, the propagation of a fault in unfractured resistant rocks can imply a high accumulation of elastic energy that may generate earthquakes of magnitudes higher than those triggered by a reactivation of previous fractures.

The Eurasian-African plate boundary in the Alboran Sea (westernmost Mediterranean) offers a unique research opportunity in a natural example that

87 can provide insights as to the propagation of fault zones (Cowie & Scholz,
88 1992) (Fig. 1). The Alboran Basin is a Neogene-Quaternary extensional basin
89 located within the Betic (Spain)-Rif (Morocco) alpine cordilleras, connected by
90 the Gibraltar Arc (Andrieux et al., 1971). The major Trans-Alboran Shear zone
91 (Larouzière et al., 1988; Frasca et al., 2015) accommodated the westward
92 displacement of the Betic-Rif orogen during the development of the Gibraltar
93 Arc. The Alboran Basin is floored by a thin continental crust made up of the
94 alpine Internal Zone metamorphic complexes, with a Variscan basement
95 located in the southeastern area (Ammar et al., 2007) resting above an
96 anomalous mantle (Hatzfeld, 1976; Comas et al., 1992). The sedimentary infill
97 consists of unconformable Miocene to Quaternary deposits (Comas et al., 1992;
98 Juan et al., 2016). This sedimentary record is mostly deformed by two
99 conjugated sets of dextral WNW-ESE and sinistral NE-SW faults, and folded by
100 ENE-WSW oriented folds (Estrada et al., 2018; Martínez-García et al., 2017),
101 the Alboran Ridge and Francesc Pagès seamount, pertaining to the main
102 antiforms (Bourgeois et al., 1992). The growth of faults and folds takes place in
103 the framework of recent NNW-SSE shortening, and regional Eurasian-African
104 plate convergence (de Mets et al., 2015). The Eurasian-African plate boundary
105 shows N-S to NW-SE convergence at present (Fadil et al., 2006; Koulali, 2011;
106 Palano et al., 2015), at a rate of 4.93 mm/yr (Argus et al., 2010). Regional
107 present-day ENE-WSW extensional stress is coeval with orthogonal
108 compression and main stress axes are inclined (de Vicente et al., 2008; Stich et
109 al., 2010).

110 The Betic-Rif Cordillera and Alboran Sea are affected by a 300 km broad
111 and heterogeneous seismicity band related to the Eurasian-African plate

boundary (Buforn et al., 1988). Seismicity generally occurs at shallow crustal levels (Buforn et al., 1995). Intermediate seismicity (40 to 120 km deep) is mainly located along a N-S elongated band in the western Alboran Basin that becomes NE-SW northwards (Morales et al., 1999; López-Casado et al., 2001; Buforn et al., 2017; Medina & Cherkaoui, 2017). Deep seismicity (600 to 640 km deep) is scarce but also occurs beneath the central Betic Cordilleras (Buforn et al., 1991, 2011). The area has heterogeneous local stresses probably due to fault interaction (Stich et al., 2010).

Several geodynamic models have been proposed for the region, including delamination (e.g. Seber et al., 1996; Lis Mancilla et al., 2013), or subduction with or without rollback (e.g. Pedrera et al., 2011; Ruiz-Constán et al., 2011; Gutscher et al., 2012; González-Castillo et al., 2015; Spakman et al., 2018), yet discussion remains alive. Moreover, in the central and eastern Alboran Sea, the recent fault system mainly composed by two conjugate WNW-ESE dextral and NNE-SSW sinistral fault sets evidences the activity of continental indentation tectonics (Estrada et al., 2018). Within this structural framework, a present-day zone of deformation with high seismic activity crossing the Alboran Sea —from Al Hoceima in the Rif to Adra and Cabo de Gata in the Betics— (Fig. 1) oblique to the previous Trans-Alboran Shear zone (Larouzière et al., 1988) has been proposed to be a main plate boundary (Fadil et al., 2006; Grevemeyer et al., 2015). However, relationships with the main tectonic structures observed in the seafloor have not yet been analysed in detail. The few available studies (Martínez-García et al., 2013; 2017 and references herein; Estrada et al., 2018) suggest that the NNE-SSW sinistral Al Idrisi Fault is the main structure with recent and present-day activity in the

137 southern Alboran Sea (Fig. 1). This fault is connected onshore with the
138 Trougout Fault in the Al Hoceima region (Morocco margin), which bounds the
139 Nekor Basin (d'Acremont et al., 2014; Lafosse et al., 2017) and its propagation
140 towards the Rif is discussed by Galindo-Zaldívar et al. (2009; 2015a) and Poujol
141 et al. (2014). The Al Hoceima region is deformed mainly by faults that determine
142 a succession of horsts and grabens, probably developed above crustal
143 detachments (Galindo-Zaldívar et al., 2009; 2015a). In the northern Alboran
144 Sea, the fault zone extends onshore toward the Campo de Dalías area,
145 connecting with the Balanegra Fault in the boundary of the Betic Cordillera and
146 Alboran Sea (Marín-Lechado et al., 2010).

147 January 25, 2016, marked the onset of a seismic sequence in the
148 central-southern Alboran Sea (www.ign.es), with a main shock of Mw=6.3 (Figs.
149 1 and 2), and whose activity continues up to 2017. The area affected extends
150 from the Francesc Pagès seamount and westernmost Alboran Ridge to the
151 Nekor Basin. The main earthquake was felt in several coastal cities of northern
152 Morocco and southern Spain, causing economic losses in both countries
153 (http://www.ign.es/resources/noticias/Terremoto_Alboran.pdf). The earthquakes
154 of this seismic sequence have been analysed in detail by the IGN (www.ign.es),
155 Buforn et al. (2017), Medina and Cherkaoui (2017) and Kariche et al. (2018).
156 They consider different velocity models for epicentre locations, suggesting that
157 activity occurred in the area nearby Al Idrisi Fault; yet they do not compare their
158 results with the more accurate position of this fault obtained by marine
159 geophysical research (Martínez-García et al., 2013; 2017; Estrada et al., 2018;
160 Lafosse et al., 2017). The comparison of seismological and marine geophysical

161 researches clearly shows that the epicentres of the earliest stage of the
162 sequence are located to the west of the Al Idrisi Fault.

163 This paper offers a multidisciplinary analysis of the recent and active
164 near-surface tectonic deformations related to the 2016-17 seismic sequence
165 within the greater context of the 1993-94 and 2004 sequences in the central
166 Alboran Sea. Our contribution provides insights into the propagation of recent
167 fault zones and how they are linked to seafloor deformations in addition to their
168 relationships with the former Al Idrisi Fault.

169

170 **2. Methodology and data**

171 The combination of different geodetic and geophysical data made it
172 possible to map the area affected by the 2016-17 seismic sequence, from the
173 deep structure to near-surface morphology as well as the overall geodynamic
174 setting.

175

176 2.1. Regional GPS data

177 Permanent GPS stations surrounding the central Alboran Sea served as
178 the reference for present-day deformation in the region. MALA and ALME
179 stations (respectively by Malaga and Almeria) along the Betic Cordillera coast,
180 and MELI (by Melilla) on the African coast, time series were obtained from the
181 EUREF permanent Network. Data were considered up to June 2017, and these
182 stations were in operatation: ALME since 2001; MALA since 2005 and MELI

since 2012. GNSS data were processed by means of Bernese Software to determine the displacement vectors.

2.2. Seismicity data

The seismicity database of the Spanish National Geographic Institute (IGN) (www.ign.es) registered the 2016-17 seismic sequence as well as the two previous main seismic series, in 1993-94 and 2004. The 2004 seismic sequence was carefully relocated by Van der Woerd et al. (2014). As the precise location of seismicity is sensitive to velocity models and to the distance of the seismic stations (Michelini & Lomax, 2004), literature (Buforn et al. 2017, Medina & Cherkaoui, 2017, Kariche et al. 2018) shows a non-coincident location for the 2016-17 seismic sequence´ epicentres. The 1993-94 and 2016-17 seismic sequences´ epicentre and hypocentre locations were calculated through a standard procedure considering the first arrivals of P and S waves and a standard velocity model (Carreño-Herrero & Valero-Zornoza, 2011). A careful relocation of the main events was provided by Buforn et al. (2017) and the IGN (IGN, 2016; www.ign.es) in light of the standard and recent velocity model (El Moudnib et al., 2015). Earthquake focal mechanisms were also obtained from the IGN database (www.ign.es), established from first arrival P-wave polarity. The present-day stress tensor was determined from seismicity using the method by Michael (1984), improved by Vavryčuk (2014).

2.3. Marine geophysics

206 The area affected by the 2016-17 seismic series was surveyed during the
207 INCRISIS cruise on board the R/V Hesperides in May, 2016. A dense grid of 31
208 survey lines, with a total length of about 900 km, was designed taking into
209 account the regional water depths and the general orientation of the
210 morphological and structural features (Fig. 1b). Data positioning was
211 determined via a Global Positioning System (GPS). The studied area was
212 covered by a multibeam SIMRAD EM120 echosounder (frequency 12 kHz) that
213 enabled us to record high resolution bathymetry. Vertical resolution was
214 approximately 0.025% of water depth. CARIS Hips software was used for
215 multibeam data processing. This bathymetry was integrated with previous
216 datasets in the area
217 (http://gma.icm.csic.es/sites/default/files/geowebs/OLsurveys/index.htm) and
218 gridded at 25 m.
219 Simultaneously with multibeam bathymetry, very high resolution seismic
220 profiles were acquired with the SIMRAD TOPAS PS18 system (frequencies of
221 18 kHz - 1 to 6 kHz). In addition to this information, multi- and single-channel
222 seismic records from the Instituto de Ciencias del Mar-CSIC database
223 (http://gma.icm.csic.es/sites/default/files/geowebs/OLsurveys/index.htm) were
224 considered (Fig. 1c). All seismic profiles were integrated into a Kingdom Suite
225 project (IHS Kingdom) for their correlation and interpretation. Likewise, gravity
226 data were obtained during the INCRISIS cruise using a Lockheed Martin BMG3
227 marine gravimeter with a precision of 0.7 mGal. Gravity Free air and Complete
228 Bouguer anomalies were determined considering a standard density of 2.67
229 g/cm^3. To extend the gravity anomalies to the shoreline we used the global free

air dataset from Sandwell et al. (2014). Directional filters (horizontal gravity gradient) were applied in order to analyse the main tectonic structures.

3. Results

The area affected by the 2016-17 seismic sequence is located in the southern sector of the Alboran Sea central part (from 125 to 1450 m water depth), from the Nekor Basin to the vicinity of Alboran Ridge and Francesc Pagès seamount (Figs. 1 and 2). The northern steep side of the Alboran Ridge gives way abruptly to the Alboran Channel, whereas that of the Francesc Pagès seamount evolves to flat-lying seafloor of the deep basin through a terraced-shaped sector that parallels the seamount.

3.1. Present-day Alboran Sea shortening from GPS data and plate deformation

Deformation within the Alboran Sea is driven in part by the NW-SE regional convergence of the Eurasian and African plates (de Mets et al., 2015). The west to west-southwestward motion of the Betic-Rif Alboran block (Koulali et al., 2011; Palano et al., 2015) may also be the result of ongoing slab rollback towards the west (Pedrera et al., 2011; Ruiz-Constán et al., 2011; Gutscher et al., 2012; González-Castillo et al., 2015; Spakman et al., 2018), which would explain the E-W to ENE-WSW extensional focal mechanisms observed in the West Alboran Sea (Stich et al., 2010). At present, the GEODVEL plate model (Argus et al., 2010) indicates a N141ºE trend of convergence at a rate of 4.93 mm/yr in this region, supported by regional GPS data (Fadil et al., 2006). This regional deformation produces a NNW-SSE shortening which, in the central part

of the Alboran Sea, may be constrained by the MALA and ALME stations in Spain, and by MELI station in Morocco (Fig. 1). The higher rates of MALA station with respect to ALME evidence ENE-WSW extension in the Betic Cordillera (Galindo-Zaldivar et al., 2015b). The southern displacement of ALME and MALA stations relative to the European plate contrasts with the northern displacement of MELI, supporting present-day shortening in the central Alboran Sea. The most intensely seismic area in 2016-17 is located in between MALA and MELI stations, with a relative NNW-SSE (N173ºE) shortening of 3.3 mm/yr.

3.2. Recentmost seismic sequence

A seismic zone of intense activity affects the central Alboran Sea, from the Campo de Dalias region in the north, to the Al Hoceima region in the south (Figs. 1 and 2), it being most intense at the southern end (Grevemeyer et al., 2015). The most recent seismic sequences were in 1993-94, 2004 and 2016-2017 (Fig. 2). The 1993-94 seismic sequence affected the coastal region nearby Al Hoceima, with a main earthquake of Mw=5.6 (May 26, 1994), after an earlier earthquake in the Campo de Dalías area, of Mw= 5.3 (Dec 23, 1993). In 2004, another seismic sequence with a devastating earthquake event of Mw= 6.4 (Feb 24) occurred onshore in the Al Hoceima region causing nearly 600 deaths and with aftershocks reaching the Alboran Sea (Van der Woerd et al., 2014). Earthquake focal mechanisms were very similar in all cases, pointing mainly to sinistral strike-slip along the NNE-SSW oriented deformation zone (El Alami et al., 1998; Stich et al., 2006, 2010), although also possible is the activity

277 of WNW-ESE dextral faults in the 2004 sequence that affect Al Hoceima
278 onshore areas (Akoglu et al., 2006; Van der Woerd et al., 2014).

279 The 2016-17 seismic sequence (Figs. 2 and 3) was initiated by a
280 moderate earthquake (Jan 21, 2016, Mw=5.1) followed closely by a stronger
281 event (Jan 25, Mw= 6.3) and by a long seismic series of decreasing activity
282 during 2016-17 (Buforn et al., 2017; Medina & Cherkaoui, 2017; Kariche et al.,
283 2018). The relatively long distances from hypocentres to seismic stations,
284 generally greater than 50 km and in some cases reaching more than 80 km,
285 decreases the quality of earthquake locations. Buforn et al. (2017) recognize
286 average horizontal errors of 5 km and vertical errors of 10 km, comprised
287 between 2 to 10 km horizontally and 3 to 17 km vertically. The location of 2016-
288 17 seismic activity established by the IGN standard terrain velocity model
289 (Carreño-Herrero & Valero-Zornoza, 2011) (Figs. 2a and 3) or El Moudnib et al.
290 (2015) velocity model (Fig. 2b) shows a deformation band with two alignments,
291 the main one, oriented NNE-SSW, changing sharply to a ENE-WSW trend.
292 Considering the IGN standard terrain velocity model (Carreño-Herrero & Valero-
293 Zornoza, 2011) (Figs. 2a and 3), the NNE-SSW alignment is about 40 km in
294 length and 10-20 km wide, and includes shallow earthquakes (< 35 km depth)
295 that affect the crust and upper mantle. It is parallel and significantly displaced
296 westwards (up to 10 km) with respect to the Al Idrisi Fault (Fig. 2). The ENE-
297 WSW alignment, about 20 km long and 10-15 km wide, is located along the
298 northern side of the westernmost Alboran Ridge and the Francesc Pagès
299 seamount, and is also characterized by a shallow seismicity (< 35 km). During
300 month 1 (Jan 2016), the seismicity clearly defines the two alignments with
301 widths of less than 10-20 km, the main southern one being displaced 5 to 10 km

302 westwards with respect to the trace of the main Al Idrisi Fault (Figs. 2 and 3a).
303 During month 2 (Feb 2016), seismic activity decreases and both alignments
304 become wider (10-20 km) (Fig. 3b). Then, from month 3 (March 2016) to
305 present, seismicity gradually decreased and affected a broader area, more than
306 15-25 km wide (Fig. 3c), in between the one clearly defined in month 1, and
307 bounded eastward by the main trace of Al Idrisi Fault. Buforn et al. (2017)
308 relocate the earthquakes considering El Moudnib et al. (2015) velocity model
309 and also obtain the same pattern formed by two alignments, the NNE-SSW with
310 a westward offset with respect to the Al Idrisi Fault seabottom location.

311 The earthquake focal mechanisms of the two seismicity alignments show
312 different behaviours (Fig. 3d). The main NNE-SSW alignment is characterized
313 by sinistral earthquake focal mechanisms related to NNE-SSW subvertical
314 faults, roughly parallel to the elongation of the alignment. There is also
315 heterogeneity of earthquake focal mechanisms with inclined P and T axes and
316 normal faults, supporting ENE-WSW extension toward the southern deformation
317 zone. In contrast, the ENE-WSW alignment is characterized by highly
318 homogeneous reverse earthquake focal mechanisms associated with ENE-
319 WSW faults. Present-day stress (Fig. 3) supports low NNW (N319ºE to N332ºE)
320 inclined compression and orthogonal horizontal extension in both segments
321 linked to prolate stress ellipsoids. Inclination is higher (47º) in the main
322 alignment and its axial ratio is closer to triaxial stress.

323

324 3.3. Deep structure from gravity data

Bouguer complete gravity anomalies decrease in the Alboran Sea, from 110 mGal to 30 mGal, in a smooth transition from the east to the west up to 4.5ºW (Casas & Carbó, 1990). As the amplitude decreases, it narrows to the west, so that the greatest values are located in the central part.

The Bouguer complete anomaly map of the 2016-17 seismic sequence area and its surroundings shows values between 100 and 10 mGal. Despite some isolated highs, the values decrease progressively from north in the central Alboran to south in the Moroccan margin. Bouguer anomaly highs in the central Alboran (northern part of Fig. 4a) support the presence of a local thinning of the continental crust (Galindo-Zaldivar et al., 1998). The shaded relief of the complete Bouguer anomaly map with illumination from the east (Fig. 4b) is sensitive to N-S trends and tracks the extension of alignments coming out of Nekor Basin, at least as far as the Alboran Ridge. One alignment (labeled “B” in Fig. 4b) nearly parallels the Al Idrisi Fault, though displaced westward. The plots of the 2016-17 epicentres of earthquakes having magnitude over 3.9, once relocated, show that the southern sector lies over the alignment located in the middle.

3.4. Recent and active near-surface tectonic and sedimentary deformations

The morpho-bathymetric and seismic analysis of the near-surface sediments affected by the 2016-17 seismic sequence provides evidence of recent and active faults, as well as folds and mass transport deposits (MTDs) (Figs. 5, 6, 7, 8 and 9). MTDs are located on the northern side of the Francesc Pagès seamount and Alboran Ridge, along the ENE-WSW active seismicity

alignment and the main earthquake (Figs. 5 and 6). Based on the thickness of remobilized sediment, small-scale MTDs (a few ms thick) and large-scale MTDs (tens of ms thick) were identified.

The small-scale MTDs occur mostly on the relatively steep slopes (~<5º) of the northern side of both seamounts, from >250 m to 1000 m water depth. They appear as vertically stacked subtabular units (a few tens of milliseconds) of unconsolidated deposits, and lenticular and irregular bodies of semi-transparent, contorted and discontinuous stratified facies, separated by relatively high reflectivity surfaces with local hyperbolic echoes. The strata pattern suggests the recurrent nature of gravity drive transport. These facies conform an irregular seafloor surface with gentle undulations (metric in scale). The large-scale MTDs mainly occur seaward with respect to the previous ones, and extend down to the deep basin (as much as 1450 m water depth). They are related to slide scars, most of them removing the small-scale MTDs. The slide scars display an amphitheatre shape (up to 1 km wide, 40 m relief) recognizable at seafloor, where they extend along a fringe at the foot of the Francesc Pagès seamount. Most of these MTDs are detached from the slide scars, and are acoustically defined by lenticular bodies (up to 55 ms thick) internally characterized by semitransparent and discontinuous stratified facies, and having a distinctive irregular seafloor surface recognized bathymetrically. Their acoustic character indicates disintegration of the removed mass, just after the initiation of mass flow-type movement. Seismic records also provide evidence of buried large-scale MTDs that interrupt and erode the surrounding basinal undeformed stratified facies, suggesting the episodic nature of such slope

374 sedimentary instabilities, at least in recent geological times. Their stratigraphic
375 position points to a simultaneous occurrence of some MTDs (Fig. 6).

376 With respect to the folds, the Alboran Ridge and Francesc Pagès
377 seamount constitute the main antiformal structures deforming the region (Figs.
378 5 and 7). The ENE-WSW folds affect Miocene age deposits (Martínez-García et
379 al., 2013). The fold geometry is irregular, with variable wavelengths (km in
380 scale) and vergences (NNW or SSE). In addition, smaller-scale folds (hundreds
381 of meters in scale) are identified in relation to the Al Idrisi Fault (Fig. 8), with
382 axes oriented parallel to it.

383 The main fracture of morphological and seismic expression, deforming
384 the most recent sediments, is the sinistral Al Idrisi Fault zone (Martínez-García
385 et al., 2011, 2013, 2017) (Figs. 5 and 8). This fault has a 50 km-long northern
386 segment with N35ºE trend. It develops a recent fault scarp of about 20 to 30
387 ms (15 to 23 m) at the northwestern edge of the Alboran Ridge that constitutes
388 the upthrown block (Figs. 5 and 8). In the hanging wall, small-scale MTDs are
389 recognized. The near-surface sediments in this sector are affected by folds. Al
390 Idrisi Fault changes its direction suddenly to N15ºE in the area between the
391 Francesc Pagès seamount and the westernmost end of the Alboran Ridge.
392 Here, it is characterized by a sharp elongated depression covered by
393 undeformed recent sediments. The main N15ºE southern segment is about 20
394 km long and extends discontinuously southward, towards the Nekor Basin in
395 relay with the Trougout Fault, forming splay faults (Lafosse et al., 2017). The
396 southern end of Al Idrisi Fault trace is located at a deformation zone with
397 smaller faults reaching the seabottom (Fig. 5). Previous research of earthquake
398 focal mechanisms (Grevemeyer et al., 2015; Martínez-García et al., 2011, 2013,

2017) suggests a sinistral slip on the Al Idrissi Fault NNE-SSW vertical fault plane, further confirmed by the short displacement, roughly 5 km, of the antiformal axis of Alboran Ridge with respect to the Francesc Pagès seamount (Martínez-García et al. 2011, 2013, 2017).

Our new geomorphological and tectonic map evidences, for the first time, a recent fault zone to the north of the Nekor Basin affected by the 2016-17 seismic sequence (Figs. 5 and 9). It is located approximately 5 to 10 km westward of the Al Idrisi Fault, south of Francesc Pagès seamount. Its bathymetric expression (a few meters of relief) correlates with the epicentral area. The faults have NW-SE orientation, with high northeastward or southwestward dips. The very high resolution seismic images of this recent fault zone suggest they are grouped in conjugate faults with a normal component affecting the most recent sediments, some of them reaching up to the seafloor (Fig. 9).

4. Discussion

This multidisciplinary focus on the 2016-17 seismic sequence in the Alboran Sea —in the wake of previous sequences in 1993-94 and 2004, and the former Al Idrisi Fault— sheds light on the seafloor deformation and relevant implications in terms of geological hazard. The results help to constrain the processes that occur during migration and propagation of active tectonic brittle deformations.

422 4.1. Constraining active tectonics: seismicity and seafloor deformations

423 Epicentres related to wrench faults are expected to be located along the fault
424 zone trace. Vertical nodal planes of earthquake focal mechanisms from the
425 main 2016 earthquake and most of the events in the southern Alboran Sea
426 undoubtedly evidence the vertical dip of the seismic active faults (Fig. 3), in
427 agreement with the seismological results of Buforn et al. (2017). Anyway,
428 aftershock sequences can affect a wide zone (e.g. >10 km wide with respect to
429 the main fault during the Landers 1992 seismic sequence, Hauksson et al.,
430 1993) favoured by the structural complexity and pre-existing structures. In spite
431 of Buforn et al. (2017) establish horizontal and vertical errors for the 2016-17
432 seismic sequence location, and Buforn et al. (2017) as well as Medina and
433 Cherkaoui (2017) relate the seismicity with the Al Idrisi Fault, the careful
434 analyses of epicentre locations for most of the NNE-SSW seismicity alignment
435 (IGN, www.ign.es; Buforn et al., 2017; Medina & Cherkaoui, 2017; Kariche et
436 al., 2018) points to they are displaced westwards with respect to the seafloor
437 trace of the Al Idrisi Fault determined by marine geophysical data (Martínez-
438 García et al., 2013, 2017; Estrada et al., 2018) (Figs. 2, 3 and 5). This
439 displacement of the earthquakes is higher when the standard velocity model
440 (Carreño-Herrero & Valero-Zornoza, 2011) is considered (IGN, www.ign.es;
441 Medina and Cherkaoui, 2017; Kariche et al., 2018): roughly 10 km for the first
442 stage earthquakes (Figs. 2a and 3a), as opposed to the roughly 5 km (Buforn et
443 al., 2017) with the model by El Moudnib et al. (2015) (Fig. 2b). Although the
444 mislocation of earthquakes by the poorly constrained velocity models and far
445 seismic stations, may produce a westward shift of the seismicity with respect to
446 the Al Idrisi Fault, all the available seismological studies (IGN, www.ign.es;

447 Buforn et al., 2017; Medina & Cherkaoui, 2017; Kariche et al., 2018) support the
448 offset to the west of the seismicity and fault activity with respect to the former Al
449 Idrisi Fault that roughly constitutes the eastern boundary of the fault zone. Our
450 findings based on the marine geophysical dataset demonstrate the
451 development of recent faults west of the former Al Idrisi Fault related to the
452 westward propagation of the deformation (Figs. 2, 3, 8, 9 and 10).

453 The early earthquakes of the 2016-17 series are clearly grouped in the
454 two relatively narrow (~10-20 km wide) NNE-SSW and ENE-WSW alignments,
455 starting with the highest magnitude event (Mw= 6.3, Jan 25) where they join
456 (Fig. 3a). The depth of seismicity is not well constrained because of the
457 variability of crustal velocities and the few and far onshore stations; still, they
458 correspond to crustal levels (<35 km depth), in agreement with Buforn et al.
459 (2017), Medina and Cherkaoui (2017) and Kariche et al. (2018). New seismic
460 faults started to develop at shallow crustal levels (roughly 5 to 10 km depth), as
461 generally occurs in continental crust (Meissner & Strehlau, 1982). If an elliptical
462 fault surface shape is considered (Watterson, 1986), the recent fault should
463 extend in depth northward and southward into the seismogenic crustal layer.
464 When deformation propagates upwards, the triggering fault is expected to reach
465 the seafloor in the NNE-SSW epicentres alignment, due to the high dip of fault
466 plane solutions in most of the earthquake focal mechanisms. According to
467 empirical fault scaling relationships (Wells & Coppersmith, 1994), the main
468 seismic event would be related to a surface rupture between 15 and 20 km and
469 might deform the area. In the 2016-17 seismic series, a recent fault zone (10-20
470 km wide) reaching up to the seafloor was recognized in the main NNE-SSW
471 seismicity alignment, south of Francesc Pagès seamount. This recent zone

472 comprises NW-SE oriented conjugated normal faults coeval with the recent
473 sedimentation, reaching different near-surface stratigraphic levels, probably
474 rotating and connecting in depth with the major recent NNE-SSW vertical
475 sinistral fault (Fig. 10). These shallow faults accommodate the NE-SW
476 extension compatible with the activity of the main wrench fault, and are in
477 agreement with crustal thinning in the Nekor Basin confirmed by Bouguer
478 gravity anomalies (Fig. 4); they would be in line with the recent normal faults
479 described by Lafosse et al. (2017) that demonstrate that the Nekor Basin is
480 floored by a set of splay faults with normal slip component related to the
481 southern prolongation of Al Idrisi Fault.

482 During later earthquakes, the 2016-17 seismic series deformation
483 extended to a broad 10-20 km-wide fault zone in the NNE-SSW alignment,
484 bounded westward by the recent faults and eastward by the Al Idrisi Fault and
485 the Alboran Ridge. Al Idrisi Fault, in contrast, only deforms discontinuously
486 near-surface sediments along the fault trace by recent or active faults and folds,
487 suggesting the recentmost activity of some segments. Although the
488 discontinuous evidences of activity may be the consequence of a seismic
489 character of Al Idrisi Fault, with segments accumulating elastic deformation
490 before the seismic rupture, alternatively they could indicate that the activity of
491 those segments has been replaced by that of other recent faults offset to the
492 west.

493 In the ENE-WSW alignment, the morphostructural pattern and
494 deformation behaviour are different. The presence of MTDs (Figs. 5 and 6) and
495 reverse earthquake focal mechanisms (Fig. 3d), and the absence of clear
496 reverse faults affecting the near-surface, would suggest the presence of blind

497 reverse faults at the core of the Alboran Ridge antiform (Fig. 10) (Martinez-
498 Garcia et al., 2013).

499 Earthquakes may be assumed to be the main mechanism triggering the
500 MTDs, deforming the near-surface sediment of the ENE-WSW alignment (Figs.
501 5 and 6) (Casas et al., 2011). The initiation of slope failure is due to cyclic
502 loading applied on the sediment and a decreasing shear strength through the
503 development of pore overpressure. Other factors, such as tectonic deformations
504 resulting in seabed, may also contribute to increasing shear stress on the slope,
505 or a decreasing sediment strength due to shearing, dilatancy and possible
506 sediment creep (Locat & Lee, 2002).

507

508 4.2. Geodynamic implications and seismic hazard

509 The former NE-SW sinistral Trans Alboran Shear Zone (Larouzière et al.,
510 1988) constituted a main tectonic structure during the Miocene, later becoming
511 inactive and overprinted by the recent NNE-SSW deformation zone (Stich et al.,
512 2006, 2010) between Campo de Dalías (Balanegra Fault) and the Al Hoceima
513 region (Trougout Fault), including the Al Idrisi Fault (Fig. 10). This evolution
514 reveals a progressive offset to the west and rotation of the central Alboran Sea
515 active deformation zone. The recent shear zone has incipient low deformation.
516 Al Idrisi Fault, which constitutes the longest fault in this deformation zone, has
517 short strike-slip, however. It is expressed by low interaction at the edge where
518 the Al Idrisi Fault orientation trace changes, and also by the short displacement
519 between the Alboran Ridge and Francesc Pagès seamount antiform axes (Fig.
520 10).

At present, seismological and GPS studies hold the active seismic zone in the central Alboran Sea to be a main weak zone related to the Eurasian-African plate boundary (Fadil et al., 2006; Grevemeyer et al., 2015; Palano et al., 2015; Buforn et al., 2017; Medina & Cherkaoui, 2017). The fact that seismicity occurred near the African coastline in 1994, with maximum magnitude of Mw= 5.6 (May 26), and later propagated towards the continent in 2004 with a main event of Mw= 6.4 in February 24 (e.g. Akoglu et al., 2006; Van der Woerd et al., 2014 and references therein) would indicate that the 2016-17 seismicity (main event Mw= 6.3) is most likely located within the same regional deformation band (Figs. 2 and 10), at its northern edge. Accordingly, the recent fault zone exhibits a segmented behaviour with the progressive reactivation of 15-20 km length stretches demonstrated by the recent seismic series (1993-94, 2004, 2016-17) (Buforn et al., 2017; Medina & Cherkaoui, 2017; Kariche et al., 2018). In the Rif, seismic faults have rupture in depth but with no clear surface expression (Galindo-Zaldívar et al., 2009 and 2015a; Van der Woerd et al., 2014). Akoglu et al. (2006) and Van der Woerd et al. (2014) show that seismicity onshore Al Hoceima region has been produced by the activity of NNE-SSW but probably also WNW-ESE conjugated faults in NNW-SSE compression and ENE-WSW orthogonal extensional stresses.

Northwards, towards the Betic Cordillera, the deformation zone is connected with the Campo de Dalías and its seismicity during the 1993-94 series (Marín-Lechado et al., 2005) (Fig. 10).

The present day stresses determined from regional seismicity studies (de Vicente et al., 2008; Stich et al., 2010) agree with the data obtained in the context of the 2016-17 seismic sequence (Figs. 3 and 10). The NW-SE

546 compression is prolate to triaxial, and inclined towards N319ºE in the NNE-SSW
547 seismicity alignment, while N332ºE in the ENE-WSW alignment, with related
548 orthogonal extension. Thus, compression is rotated in the two alignments, and
549 is compatible with sinistral fault kinematics (Fig. 10). Whereas at the Earth´s
550 surface, main stresses should be horizontal or vertical due to an absence of
551 shear stress (Anderson, 1951; Bott, 1959), the inclination of main compression
552 towards the NW at crustal depths suggests activity of northwestward thrusting
553 to some extent. Moreover, this setting could be a consequence of the presence
554 of a low-deformed resistant domain attached to the African plate, here
555 corresponding to the external Rif units on the Variscan basement (Pedrera el
556 al., 2011; Galindo-Zaldívar et al., 2015a; Estrada et al., 2018).

557 There is furthermore some disagreement between the maximum
558 horizontal compression (between N139ºE and N152ºE) and maximum local
559 shortening (N173ºE) (Fig. 10), estimated by the MALA and MELI GPS stations
560 across the seismic active area. It may be that fault activity is not due to a simple
561 strike-slip fault driven by a far field stress in the sense of Anderson (1951), but
562 could accommodate crustal block displacement. The NE-SW extension that
563 occurs towards the fault tips, at the northern edge of Campo de Dalías normal
564 faults (Marín-Lechado et al., 2005; Galindo-Zaldívar et al., 2013), is transferred
565 towards the southern edge, where normal faults splay at the Nekor Basin (Fig.
566 10) (Galindo-Zaldívar et al., 2009; Lafosse et al., 2017) and crustal thinning is
567 confirmed by gravity results (Fig. 4a).

568 The epicentres of three seismic series are located west of the main faults
569 recognized at surface, both in the Alboran Sea (Al Idrisi Fault) and in the
570 northern Rif (Trougout Fault) (Figs. 2 and 10) (Galindo-Zaldívar et al., 2009,

571 2015a; d'Acremont et al., 2014). Hence, the development of the seismic active
572 fault zone west of the well exposed Al Idrisi and Trougout faults might be
573 attributed to the growth of recent faults owing to westward migration (Vitale et
574 al., 2015) of the deformation during development of the Gibraltar Arc.

575 The westward migration of the Gibraltar Arc is well constrained by
576 geological (Crespo-Blanc et al., 2016) and GPS data (Fadil et al., 2006; Koulali
577 et al., 2011; Palano et al., 2015). However, the driving mechanism remains a
578 matter of debate, with geodynamic models considering delamination (e.g. Seber
579 et al., 1996; Lis Mancilla et al., 2013) and subduction (e.g. Pedrera et al., 2011;
580 Ruiz-Constán et al., 2011; Gutscher et al., 2012; González-Castillo et al., 2015;
581 Spakman et al., 2018), while roll-back is a suitable mechanism for Gibraltar Arc
582 westward displacement and Alboran Sea development. The growth of this
583 seismic NNE-SSW fault zone occurs in the area of weakest and most
584 attenuated continental crust, corresponding to the central Alboran Sea,
585 bounded by the thick continental crust of the Betic and Rif cordilleras. In this
586 regional setting, the Eurasian-African convergence developed indentation
587 tectonics (Estrada et al., 2018) accommodated by the Al Idrisi fault zone, which
588 now extends to westward areas.

589 The development of active fault zones has vast implications for seismic
590 hazard. The reactivation of an existing fracture calls for shear stress on the
591 surface to attain the value of the friction and cohesion (Bott, 1959). Immediately
592 previous to the formation of new fractures, shear stress would have to be above
593 the values of friction in addition to cohesion —considerably higher (Anderson,
594 1951; Hajiabdolmajid et al., 2002). Given the same background setting, the
595 development of a recent fault zone would allow for the accumulation of higher

596 elastic deformation at the fault edges than along a well-developed previous
597 fracture. These factors determine that the propagation of a recent fault, as
598 occurs in the southern Alboran Sea, can produce earthquakes of higher
599 magnitudes than pre-existing faults. The highest magnitude earthquakes of
600 2004 (Galindo-Zaldívar et al., 2009; d'Acremont et al., 2014) and 2016-17
601 occurred in areas of recently developed fault segments with scarce evidence of
602 deformation at the surface (Fig. 10). Such faults tend to be particularly active in
603 their initial stage of development, entailing high seismic hazard, and are
604 moreover difficult to detect because of the low amount of accumulated
605 deformation due to their recent age.

606

607 **5. Conclusions**

608 The Alboran Sea 2016-17 seismic sequence constitutes a unique
609 opportunity to analyse the development of recent faults in conjunction with
610 seismic hazard. This sequence occurred in the southern part of an active
611 deformation zone crossing the central Alboran Sea and had a main event
612 (Mw=6.3, Jan 25, 2016) located along the corner between the NNE-SSW and
613 ENE-WSW deformation alignments, which are 10-20 km wide. The 40 km-long
614 NNE-SSW alignment is located in the Nekor Basin and Francesc Pagès
615 seamount, west of the seabottom Al Idrisi Fault trace, and the ENE-WSW one is
616 along the northern side of Alboran Ridge and Francesc Pagès seamount. Data
617 recorded during the INCRISIS cruise reveal that the ENE-WSW alignment is
618 mainly characterized by recurrent MTDs that could be linked to earthquake and
619 tectonic activity owing to uplift of the Alboran Ridge and Francesc Pagés

antiforms. The NNE-SSW seismicity alignment is related to deep vertical sinistral faults, demonstrated by earthquake focal mechanisms, offset 5 to 10 km westwards from the former Al Idrisi Fault. The major NNE-SSW deep sinistral fault zone responsible for the 2016-17 main events would have activated fault segments up to 15 to 20 km in length for single events. The INCRISIS cruise reveals evidence for recent near-surface ruptures in NW-SE normal faults. These recent faults are related to the western boundary of the deformation zone, bounded eastward by the Al Idrisi Fault; although it is the main fault with seafloor expression, it has segments without recent activity. The present-day stress from earthquake focal mechanisms of 2016-17 constrains a maximum prolate to triaxial compression inclined towards N319ºE in the NNE-SSW alignment, and N332ºE in the ENE-WSW alignment, with related orthogonal extension. Stresses are oblique to the N173ºE shortening determined by GPS data that support sinistral slip behaviour, with some extent of northwestward thrusting.

These data reveal a westward migration and offset of active deformation with respect to the already developed Al Idrisi Fault (Fig. 10) that may be linked to the westward development of the Gibraltar Arc. Moreover, the NNE-SSW deformation zone is segmented and was progressively reactivated near the African coast in the 1993-94 seismic sequence, the southern onshore part being affected in 2004 and probably activating NNE-SSW sinistral and WNW-ESE dextral faults, with deformation later propagating offshore toward the northeast in 2016-17. The present-day NW-SE Eurasian-African plate convergence in the westernmost Mediterranean and the inherited heterogeneous rigid basement structures determine the location of deformation areas. At present, a main NNE-

645 SSW sinistral deformation fault zone, including the Al Idrisi Fault and recent
646 developed faults offset to the west, connects the NW-SE extensional faults of
647 the Campo de Dalias´s northern edge (Betic Cordillera) with the southern
648 edge´s normal splay faults located at the Nekor Basin in the Rif (Fig. 10). This
649 setting also contributes to the local crustal thinning of Nekor Basin supported by
650 gravity data.

651 Geological hazard in the central Alboran Sea is closely related to the
652 seismicity that constitutes a main triggering mechanism of MTDs and is
653 moreover responsible for coseismic seafloor displacements. The development
654 of recent faults that condition the westward widening of the fault zone compared
655 with the already developed faults would imply the activity of the largest
656 segments and the greatest accumulation of elastic energy, producing high
657 magnitude earthquakes that increase seismic hazard. In any case, low
658 accumulated deformation and recent activity are predominant features making it
659 possible to recognize such faults, and therefore deserving further analysis
660 through a multidisciplinary approach.

661

662 **Acknowledgements**

663 We acknowledge the comments of Prof. N. Niemi, Prof. J. Bruce H.
664 Shyu, Prof. M-A Gutscher and three anonymous reviewers which served to
665 improve the quality of this paper. We also thank A. Mandarieta for his help with
666 the figures. The geological data referenced in this paper are available in the
667 text, the seismicity data are available on the IGN website at
668 http://www.ign.es/web/ign/portal/sis-catalogo-terremotos and the marine

669 geophysical data are available on the ICM-CSIC website at
670 http://gma.icm.csic.es/sites/default/files/geowebs/OLsurveys/index.htm . This
671 study was supported by the Spanish projects INCRISIS (CGL2016-80687-R
672 AEI/FEDER) DAMAGE Project FEDER, SARAS and FAUCES (CTM2015-
673 65461-C2-1-R) and Marlboro cruises. French program Actions Marges, the
674 EUROFLEETS program (FP7/2007-2013; n°228344). The participation of D.
675 Palomino and J.T. Vazquez was funded by the IEO project RIGEL.

676

677 **References**

678 Akoglu, A.M., Cakir, Z., Meghraoui, M., Belabbes, S., El Alami, S.O., Ergintav,
679 S., & Akyüz, H.S. (2006). The 1994–2004 Al Hoceima (Morocco)
680 earthquake sequence: Conjugate fault ruptures deduced from InSAR,
681 *Earth Planet. Sci. Lett.,* 252, 467-480, doi: 10.1016/j.epsl.2006.10.010.

682 Ammar, A., Mauffret, A., Gorini, C., & Jabour, H. (2007). The tectonic structure
683 of the Alboran Margin of Morocco, *Rev. Soc. Geol. Esp*., 20, 247-271.

684 Anderson, E.M. (1951), *The dynamics of faulting and dyke formation with*
685 *applications to Britain*, Hafner Pub. Co.

686 Andrieux, J., Fontbote, J.M., & Mattauer, M. (1971). Sur un modèle explicatif de
687 l'Arc de Gibraltar, *Earth Planet. Sci. Lett.*, 12, 191-198.

688 Argus, D.F., Gordon, R.G., Heflin, M.B., Ma, C., Eanes, R.J., Willis, P., …
689 Owen, S.E. (2010). The angular velocities of the plates and the velocity
690 of Earth's centre from space geodesy, *Geophys. J. Intern.*, 180, 913-
691 960, doi: 10.1111/j.1365-246X.2009.04463.x.

692 Bott, M.H.P. (1959). The mechanics of oblique slip faulting, *Geol. Mag.*, 96,
693 109-117.

694 Bourgois, J., Mauffret, A., Ammar, A., & Demnati, A. (1992). Multichannel
695 seismic data imaging of inversion tectonics of the Alboran Ridge
696 (Western Mediterranean Sea), *Geo-Mar. Lett.*, 12, 117-122.

697 Buforn, E., Sanz de Galdeano, C., & Udías, A. (1995). Seismotectonics of the
698 Ibero-Maghrebian region, *Tectonophysics*, 248, 247-261.

699 Buforn, E., Udias, A., & Madariaga, R. (1991). Intermediate and deep
700 earthquakes in Spain, in *Source Mechanism and Seismotectonics,*
701 edited by A. Udías & E. Buforn, pp. 375-393, Springer, Birkhäuser,
702 Basel.

703 Buforn, E., Pro, C., Cesca, S., Udias, A., & del Fresno, C. (2011). The 2010
704 Granada, Spain, deep earthquake. *Bulletin of the Seismological Society*
705 *of America*, 101(5), 2418-2430.

706 Buforn, E., Pro, C., Sanz de Galdeano, C., Cantavella, J.V., Cesca, S.,
707 Caldeira, B., … Mattesini, M. (2017). The 2016 south Alboran
708 earthquake (Mw=6.4): A reactivation of the Ibero-Maghrebian region?,
709 *Tectonophysics*, 712, 704-715, doi: 10.1016/j.tecto.2017.06.033.

710 Carreño-Herrero, E., & Valero-Zornoza, J.F. (2011). Sismicidad de la Península
711 Ibérica en el periodo instrumental: 1985-2011, *Ense. Cienc. Tier.*, 19,
712 289-295.

713 Casas, A., & Carbo, A. (1990). Deep structure of the Betic Cordillera derived
714 from the interpretation of a complete Bouguer anomaly map, *J.*
715 *Geodynamics*, 12, 137-147.

716 Casas, D., Ercilla, G., Yenes, M., Estrada, F., Alonso, B., García, M., &
717 Somoza, L. (2011). The Baraza Slide: model and dynamics, *Mar.*
718 *Geophys. Res.,* 32, 245-256, doi: 10.1007/s11001-011-9132-2.

719 Comas, M., García-Dueñas, V., & Jurado, M. (1992). Neogene tectonic
720 evolution of the Alboran Sea from MCS data, *Geo-Mar. Lett.*, 12, 157-
721 164.

722 Cowie, P.A., & Scholz, C.H. (1992). Growth of faults by accumulation of seismic
723 slip, *J. Geophys. Res., Solid Earth,* 97, 11085-11095.

724 Crespo-Blanc, A., Comas, M., & Balanyá, J. C. (2016). Clues for a Tortonian
725 reconstruction of the Gibraltar Arc: Structural pattern, deformation
726 diachronism and block rotations. *Tectonophysics*, 683, 308-324.

727 d' Acremont, E., Gutscher, M.A., Rabaute, A., Mercier de Lépinay, B., Lafosse,
728 M., Poort, J. … Gorini, C. (2014). High-resolution imagery of active
729 faulting offshore Al Hoceima, Northern Morocco, *Tectonophysics*, 632,
730 160-166, doi: 10.1016/j.tecto.2014.06.008

731 de Mets, C., Laffaldano, G., & Merkouriev, S. (2015). High-resolution Neogene
732 and Quaternary estimates of Nubia-Eurasia-North America Plate
733 motion, Geophys. *J. Int.,* 203, 416-427, doi: 10.1093/gji/ggv277.

734 de Vicente, G., Cloetingh, S., Muñoz-Martín, A., Olaiz, A., Stich, D., Vegas, R.,
735 … Fernández-Lozano, J. (2008). Inversion of moment tensor focal

736 mechanisms for active stresses around the microcontinent Iberia:
737 Tectonic implications, *Tectonics*, 27, TC1009, doi:
738 10.1029/2006TC002093.

739 El Alami, S.O., Tadili, B.A., Cherkaoui, T.E., Medina, F., Ramdani, M., Brahim,
740 L.A., & Harnafi, M. (1998). The Al Hoceima earthquake of May 26, 1994
741 and its aftershocks: a seismotectonic study, *Ann. Geophys.*, 41, 519-
742 537.

743 El Moudnib, L., Villaseñor, A., Harnafi, M., Gallart, J., Pazos A., Serrano, I., …
744 Chourak, M. (2015). Crustal structure of the Betic–Rif system, western
745 Mediterranean, from local earthquake tomography, *Tectonophysics,*
746 643, 94-105, doi: 10.1016/j.tecto.2014.12.015

747 Estrada, F., Galindo-Zaldívar, J., Vázquez, J.T., Ercilla, G., D'Acremont, E.,
748 Alonso, B., & Gorini, C. (2018). Tectonic indentation in the central
749 Alboran Sea (westernmost Mediterranean), *Terra Nova*, 30, 24-33, doi:
750 DOI: 10.1111/ter.12304

751 Fadil, A., Vernant, P., McClusky, S., Reilinger, R., Gomez, F., Sari, D.B., ...
752 Barazangi, M. (2006). Active tectonics of the western Mediterranean:
753 Geodetic evidence for rollback of a delaminated subcontinental
754 lithospheric slab beneath the Rif Mountains, Morocco, *Geology*, 34,
755 529-532, doi: 10.1130/G22291.1.

756 Frasca, G., Gueydan, F., & Brun, J.P. (2015). Structural record of Lower
757 Miocene westward motion of the Alboran Domain in the Western Betics,
758 Spain, *Tectonophysics*, *657*, 1-20.

759 Galindo-Zaldivar, J., Gonzalez-Lodeiro, F., Jabaloy, A., Maldonado, A., &
760 Schreider, A. (1998). Models of magnetic and Bouguer gravity
761 anomalies for the deep structure of the central Alboran Sea basin, *Geo-*
762 *Mar. Lett.*, 18, 10-18.

763 Galindo-Zaldívar, J., Chalouan, A., Azzouz, O., Sanz de Galdeano, C.,
764 Anahnah, F., Ameza, L., … Chabli, A. (2009). Are the seismological
765 and geological observations of the Al Hoceima (Morocco, Rif) 2004
766 earthquake (M=6.3) contradictory?, *Tectonophysics,* 475, 59-67, doi:
767 10.1016/j.tecto.2008.11.018.

768 Galindo-Zaldívar, J., Azzouz, O., Chalouan, A., Pedrera, A., Ruano, P., Ruiz-
769 Constán, A., … Benmakhlouf, M. (2015a). Extensional tectonics,
770 graben development and fault terminations in the eastern Rif (Bokoya–
771 Ras Afraou area), *Tectonophysics*, 663, 140-149 doi:
772 10.1016/j.tecto.2015.08.029.

773 Galindo-Zaldivar, J., Gil, A.J., Sanz de Galdeano, C., Lacy, M.C., García-
774 Armenteros, J.A., Ruano, P., … Alfaro, P. (2015b). Active shallow
775 extension in central and eastern Betic Cordillera from CGPS data,
776 *Tectonophysics*, 663, 290-301, doi: 10.1016/j.tecto.2015.08.035.

777 Gonzalez-Castillo, L., Galindo-Zaldivar, J., de Lacy, M., Borque, M., Martinez-
778 Moreno, F., García-Armenteros, J., & Gil, A. (2015). Active rollback in
779 the Gibraltar Arc: Evidences from CGPS data in the western Betic
780 Cordillera. *Tectonophysics*, 663, 310-321.

781 Grevemeyer, I., Gràcia, E., Villaseñor, A., Leuchters, W., & Watts, A.B. (2015).
782 Seismicity and active tectonics in the Alboran Sea, Western

783 Mediterranean: Constraints from an offshore-onshore seismological
784 network and swath bathymetry data, *J. Geophys. Res.: Solid Earth*,
785 120, 8348-8365, doi: 10.1002/2015JB012073.

786 Gutscher, M. A., Dominguez, S., Westbrook, G. K., Le Roy, P., Rosas, F.,
787 Duarte, J. C., . . . Bartolome, R. (2012). The Gibraltar subduction: A
788 decade of new geophysical data. *Tectonophysics*, 574-575, 72-91.
789 doi:https://doi.org/10.1016/j.tecto.2012.08.038

790 Hajiabdolmajid, V., Kaiser, P. K., & Martin, C. D. (2002). Modelling brittle failure
791 of rock, *International Journal of Rock Mechanics and Mining Sciences*,
792 *39*(6), 731-741.

793 Hatzfeld, D. (1976). Deep-structure of Alboran Sea. *C. R. hebd. Seanc. Acad.*
794 *Sci.*, D283, 1021-1024.

795 Hauksson, E., Jones, L. M., Hutton, K., & Eberhart-Phillips, D. (1993). The 1992
796 Landers earthquake sequence: Seismological observations. *Journal of*
797 *Geophysical Research: Solid Earth, 98*(B11), 19835-19858.

798 IGN, (2016). Informe de la actividad sísmica en el Mar de Alborán 2016
799 (http://www.ign.es/resources/noticias/Terremoto_Alboran.pdf). *Instituto*
800 *Geográfico Nacional – Red Sísmica Nacional*, 1-14.

801 Juan, C., Ercilla, G., Hernández-Molina, J.F., Estrada, F., Alonso, B., Casas, …
802 Ammar, A. (2016). Seismic evidence of current-controlled
803 sedimentation in the Alboran Sea during the Pliocene and Quaternary:
804 Palaeoceanographic implications, *Mar. Geol.,* 378, 292-311, doi :
805 10.1016/j.margeo.2016.01.006.

806 Kariche, J., Meghraoui, M., Timoulali, Y., Cetin, E. & Toussaint, R. (2018). The
807 Al Hoceima earthquake sequence of 1994, 2004 and 2016: Stress
808 transfer and poroelasticity in the Rif and Alboran Sea region, *Geophys.*
809 *J. Inter.*, *212*(1), 42-53.

810 Koulali, A., Ouazar, D., Tahayt, A., King, R. W., Vernant, P., Reilinger, R. E., . . .
811 Amraoui, N. (2011). New GPS constraints on active deformation along
812 the Africa–Iberia plate boundary. *Earth and Planetary Science Letters*,
813 308(1), 211-217. doi:https://doi.org/10.1016/j.epsl.2011.05.048

814 Lafosse, M., d'Acremont, E., Rabaute, A., Mercier de Lépinay, B., Tahayt, A.,
815 Ammar, A. & Gorini, C. (2017). Evidence of Quaternary transtensional
816 tectonics in the Nekor basin (NE Morocco), *Basin Res.*, 29, 470–489,
817 doi : 10.1111/bre.12185.

818 Larouzière, F., Bolze, J., Bordet, P., Hernandez, J., Montenat, C. & Ott
819 d'Estevou, P. (1988). The Betic segment of the lithospheric Trans-
820 Alboran shear zone during the Late Miocene, *Tectonophysics,* 152, 41-
821 52.

822 Lis Mancilla, F. d., Stich, D., Berrocoso, M., Martín, R., Morales, J., Fernandez-
823 Ros, A., . . . Pérez-Peña, A. (2013). Delamination in the Betic Range:
824 Deep structure, seismicity, and GPS motion. *Geology*, 41(3), 307-310.

825 Locat, J. & Lee, H.J. (2002). Submarine landslides: advances and challenges,
826 *Can. Geotech. J.*, 39, 193-212.

827 Lopez-Casado, C., Sanz de Galdeano, C., Palacios, S. M., & Romero, J. H.
828 (2001). The structure of the Alboran Sea: an interpretation from
829 seismological and geological data. *Tectonophysics*, 338, 79-95.

830 Marín-Lechado, C., Galindo-Zaldívar, J., Gil, A.J., Borque, M.J., De Lacy, M.C.,
831 Pedrera, A., … Sanz de Galdeano, C. (2010). Levelling Profiles and a
832 GPS Network to Monitor the Active Folding and Faulting Deformation in
833 the Campo de Dalias (Betic Cordillera, Southeastern Spain), *Sensors,*
834 10, 3504, doi: 10.3390/s100403504.

835 Marín-Lechado, C., Galindo-Zaldívar, J., Rodríguez-Fernández, L.R., Serrano,
836 I., & Pedrera, A. (2005). Active faults, seismicity and stresses in an
837 internal boundary of a tectonic arc (Campo de Dalías and Níjar,
838 southeastern Betic Cordilleras, Spain), *Tectonophysics*, 396, 81-96, doi:
839 10.1016/j.tecto.2004.11.001.

840 Martínez-García, P., Soto, J.I., & Comas, M. (2011). Recent structures in the
841 Alboran Ridge and Yusuf fault zones based on swath bathymetry and
842 sub-bottom profiling: evidence of active tectonics, *Geo-Mar. Lett.,* 31,
843 19-36, doi: 10.1007/s00367-010-0212-0.

844 Martínez-García, P., Comas, M., Soto, J.I., Lonergan, L., & Watts A. (2013).
845 Strike-slip tectonics and basin inversion in the Western Mediterranean:
846 the Post-Messinian evolution of the Alboran Sea, *Basin Res.,* 25, 361-
847 387, doi: 10.1111/bre.12005.

848 Martínez-García, P., Comas, M., Lonergan, L., & Watts, A. B. (2017). From
849 Extension to Shortening: Tectonic Inversion Distributed in Time and

Space in the Alboran Sea, Western Mediterranean, *Tectonics*, 36, doi: 10.1002/2017TC004489

Medina, F., & Cherkaoui, T.E. (2017). The South-Western Alboran Earthquake Sequence of January-March 2016 and Its Associated Coulomb Stress Changes, *Open J. Earth. Res.,* 6, 35, doi: 10.4236/ojer.2017.61002.

Meissner, R., & Strehlau, J. (1982). Limits of stresses in continental crusts and their relation to the depth-frequency distribution of shallow earthquakes, *Tectonics*, 1, 73-89.

Michael, A.J. (1984). Determination of stress from slip data: faults and folds, *J. Geophys. Res.: Solid Earth*, 89, 11517-11526.

Michelini, A., & Lomax, A. (2004). The effect of velocity structure errors on double-difference earthquake location, *Geophys. Res. Lett.,* 31, L09602, doi: 10.1029/2004GL019682.

Morales, J., Serrano, I., Jabaloy, A., Galindo-Zaldivar, J., Zhao, D., Torcal, F., … Gonzalez-Lodeiro, F. (1999). Active continental subduction beneath the Betic Cordillera and the Alboran Sea, *Geology*, 27, 735-738.

Palano, M., González, P. J., & Fernández, J. (2015). The Diffuse Plate boundary of Nubia and Iberia in the Western Mediterranean: Crustal deformation evidence for viscous coupling and fragmented lithosphere. *Earth and Planetary Science Letters*, 430, 439-447. doi:https://doi.org/10.1016/j.epsl.2015.08.040

Pedrera, A., Ruiz-Constán, A., Galindo-Zaldívar, J., Chalouan, A., Sanz de Galdeano, C., Marín-Lechado, C., … González-Castillo, L. (2011). Is

there an active subduction beneath the Gibraltar orogenic arc? Constraints from Pliocene to present-day stress field. *J. Geodyn*., 52, 83-96, doi : 10.1016/j.jog.2010.12.003.

Poujol, A., Ritz, J.F., Tahayt, A. Vernant, P., Condomines, M., Blard, P.H., ... Hni, L. (2014). Active tectonics of the Northern Rif (Morocco) from geomorphic and geochronological data, *J. Geodyn*, 77, 70-88, doi: 10.1016/j.jog.2014.01.004.

Ruiz-Constán, A., Galindo-Zaldívar, J., Pedrera, A., Celerier, B., & Marín-Lechado, C. (2011). Stress distribution at the transition from subduction to continental collision (northwestern and central Betic Cordillera). *Geochemistry, Geophysics, Geosystems*, 12(12).

Sandwell, D.T., Müller, R.D., Smith, W.H., Garcia, E., & Francis, R. (2014). New global marine gravity model from CryoSat-2 and Jason-1 reveals buried tectonic structure, *Science*, 346, 65-67, doi: 10.1126/science.1258213.

Scholz, C. H. (2002). *The mechanics of earthquakes and faulting*, Cambridge university press.

Sibson, R. (1977). Fault rocks and fault mechanisms, *J. Geol. Soc.*, 133, 191-213.

Spakman, W., Chertova, M. V., van den Berg, A., & van Hinsbergen, D. J. J. (2018). Puzzling features of western Mediterranean tectonics explained by slab dragging. *Nature Geoscience, 11*(3), 211-216. doi:10.1038/s41561-018-0066-z

895 Stich, D., Serpelloni, E., de Lis Mancilla, F., & Morales, J. (2006). Kinematics of
896 the Iberia–Maghreb plate contact from seismic moment tensors and
897 GPS observations, *Tectonophysics*, 426, 295-317., doi:
898 10.1016/j.tecto.2006.08.004.

899 Stich, D., Martín, R., & Morales, J. (2010). Moment tensor inversion for Iberia–
900 Maghreb earthquakes 2005–2008. *Tectonophysics*, 483(3), 390-398.
901 doi:https://doi.org/10.1016/j.tecto.2009.11.006

902 Van Der Woerd, J., Dorbath, C., Ousadou, F., Dorbath, L., Delouis, B., Jacques,
903 E., . . . Frogneux, M. (2014). The Al Hoceima Mw 6.4 earthquake of 24
904 February 2004 and its aftershocks sequence. *Journal of Geodynamics*,
905 77, 89-109.

906 Vavryčuk, V. (2014). Iterative joint inversion for stress and fault orientations
907 from focal mechanisms, *Geophys. J. Int.*, 199, 69-77, doi:
908 10.1093/gji/ggu224

909 Vitale, S., Zaghloul, M.N., El Ouaragli, B., Tramparulo, F.D.A., & Ciarcia, S.
910 (2015). Polyphase deformation of the Dorsale Calcaire Complex and
911 the Maghrebian Flysch Basin Units in the Jebha area (Central Rif,
912 Morocco): New insights into the Miocene tectonic evolution of the
913 Central Rif belt, *J. Geodyn.*, 90, 14-31, doi: 10.1016/j.jog.2015.07.002

914 Watterson, J. (1986). Fault dimensions, displacements and growth, *Pure Appl.*
915 *Geophys.*, 124, 365-373.

916 Wells, D.L., & Coppersmith, K. J. (1994). New empirical relationships among
917 magnitude, rupture length, rupture width, rupture area, and surface
918 displacement, *Bull. Seism. Soc. Am.*, 84, 974-1002.

919

Figure captions

Fig. 1. Geological setting including regional faults and seismicity. a, Plate boundaries in the Azores-Gibraltar area (modified from Galindo-Zaldívar et al., 2003) and geological sketch of the main structural features and basins of the Alboran Sea (modified from Comas et al., 1999). Displacement of GPS stations around the Alboran Sea with respect to stable Eurasia are indicated (red arrows). The dotted area within the inset indicates the deformation area. b, Tracklines of multibeam, very high resolution seismics (TOPAS) and gravity surveyed simultaneously during the INCRISIS cruise. c, Tracklines of single- and multi-channel seismics (airguns) from the ICM database (http://gma.icm.csic.es/sites/default/files/geowebs/OLsurveys/index.htm). Legend: AF, Al Idrisi Fault; AR, Alboran Ridge; AC, Alboran Channel; BF, Balanegra Fault; CD, Campo de Dalías; CG, Cabo de Gata; CF, Carboneras Fault; DB, Djibouti Bank; EAB, East Alboran Basin; FP, Francesc Pagès seamount; NB, Nekor Basin; NF, Nekor Fault; SAB, South Alboran Basin; TF, Trougout Fault; WAB, West Alboran Basin; YF, Yusuf Fault.

Fig. 2. Seismicity distribution during the 2016-17 seismic sequence and other recent seismicity (including 1993-94 and 2004 series) (2004 seismic sequence from Van der Woerd et al., 2014; other seismicity from www.ign.es database). a, Epicentres considering a standard velocity model. b, Relocated epicentres for the highest magnitude earthquakes of the 2016-17 seismic sequence according to El Moudnib et al. (2015). Legend: FP, Francesc Pagès seamount; NB, Nekor Basin.

Fig. 3. Seismicity during the 2016-17 seismic sequence. a, Epicentres month 1 (January 2016). b, Epicentres month 2 (Feburary 2016). c, Late epicentres (March 2016 to June 2017). d, Earthquake focal mechanisms from 2016-17 seismic crisis (data from I.G.N., www.ign.es). NNE-SSW alignment in blue, ENE-WSW alignment in red. The main earthquake, located at the edge of the two alignments, is shared by the two groups. Present-day stress is determined in the two main sectors of 2016-17 Alboran Sea seismic crisis area (by the methods of Michael, 1984; improved by Vavryčuk, 2014). e, cross sections of seismic activity orthogonal to the main alignments.

Fig. 4. Gravity anomaly maps and main tectonic features. a, Bathymetry map, contour lines every 100 m. b, Complete Bouguer gravity anomaly map at 2 km resolution. Contour lines every 5 mGal. c, A shaded relief map (illuminated from the East) of the complete Bouguer gravity anomaly. Black dashed lines denote offshore N-S alignments (labeled as A, B and C); white dots mark earthquakes with magnitude > 3.9; thin contour lines represent bathymetry.

Fig. 5. Recent sea bottom deformation affecting the 2016-17 Alboran Sea seismic active area: MTDs, faults and folds. a, INCRISIS bathymetry integrated with previous datasets in the area (http://gma.icm.csic.es/sites/default/files/geowebs/OLsurveys/index.htm). Data is gridded at a resolution of 25 m. b, detailed view of recent fault scarps mapped during the INCRISIS multibeam bathymetry. The grey plain areas were not covered by the multibeam echosounder. c, geomorphological and tectonic map. The INCRISIS TOPAS seismic profiles were also integrated with the multi- and single-channel seismic records from the Instituto de Ciencias del Mar-CSIC database

968 (http://gma.icm.csic.es/sites/default/files/geowebs/OLsurveys/index.htm). 2016
969 seismicity from www.ign.es database.

970 Fig. 6. Segments of TOPAS seismic records displaying the small- and large-
971 scale MTDs mapped in the ENE-WSW seismicity alignment. Thin vertical
972 discontinuous lines, noise.

973 Fig. 7. Segments of multi-channel seismic records displaying the Alboran Ridge
974 (a) and Francesc Pagès seamount (b) folds.

975 Fig. 8. Segments of TOPAS seismic records displaying the Al Idrisi Fault
976 deformation along its trace. The fault generally affects recent sediments,
977 although undeformed sediments cover the central part of the fault trace. Thin
978 vertical discontinuous lines, noise.

979 Fig. 9. Segments of TOPAS seismic records displaying the recent fault zone
980 identified in this study. This zone is located 5 to 10 km westwards of the Al Idrisi
981 Fault (d). Thin vertical discontinuous lines, noise.

982 Fig. 10. Sketch illustrating the westward propagation of recent tectonic and
983 seismic activity in the main NNE-SSW deformation zone crossing the Alboran
984 Sea. a, Seismicity, main active structures, stress and shortening. 2004 seismic
985 sequence from Van der Woerd et al. (2014); other seismicity from www.ign.es
986 database. b, Sketch of main tectonic structures and westward migration of
987 deformation from main Al Idrisi Fault trace. c, Interpretative cross sections and
988 seismicity orthogonal to the main earthquake alignments. 1, sinistral fault (map
989 and cross section). 2, normal fault. 3, recent normal fault. 4, epicentre of main
990 event (Mw=6.3, Jan 25, 2016). 5, Active blind thrust. 6, Active NNE-SSW
991 sinistral deep vertical crustal fault segment bounding westwards the NNE-SSW

992 2016-17 seismicity alignment. 7, Active NNE-SSW vertical sinistral crustal fault
993 segment related to the 1993-94 seismic crisis. 8, Active NNE-SSW vertical
994 sinistral crustal fault segment related to the 2004 seismic crisis. 9, Offset to the
995 west of recent deformation and seismicity in respect to Al Idrisi Fault. 10,
996 Estimated convergence trend from GPS data. 11, Regional plate convergence
997 trend. 12, Present-day trends of compression and extension determined from
998 earthquake focal mechanisms. FP, Francesc Pagès seamount. MTD, Mass
999 transport deposits.

1000

Fig. 1.

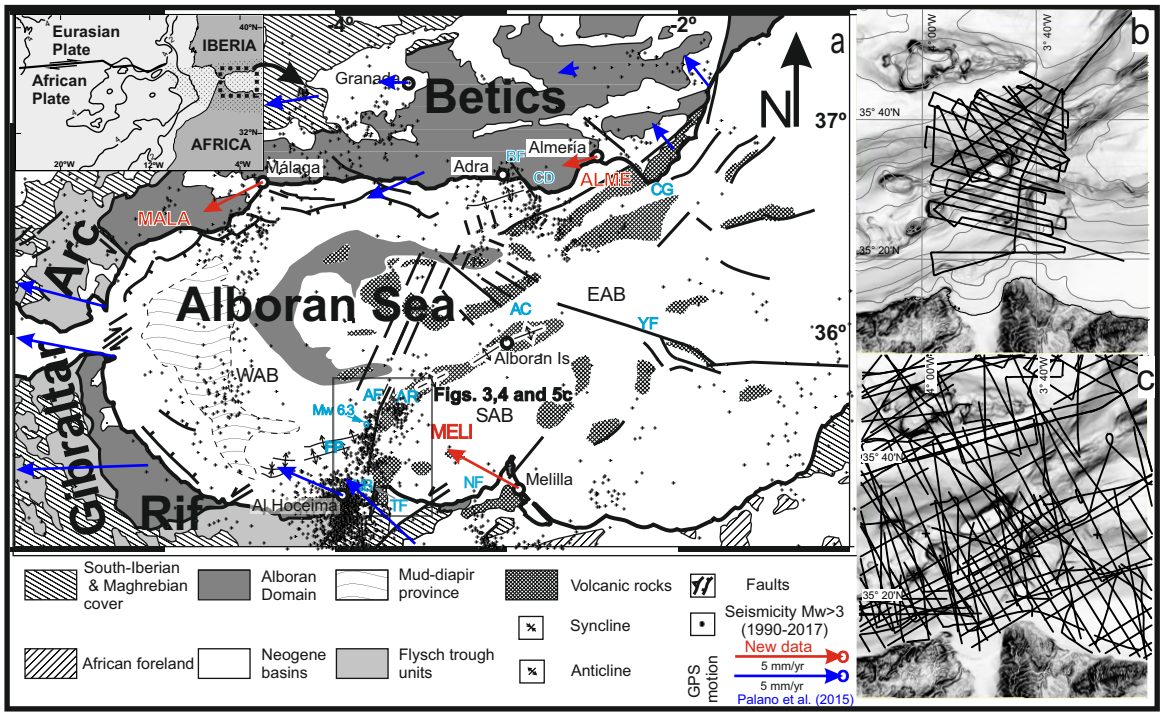
Eurasian Plate
African Plate
IBERIA
AFRICA
Granada
Betics
Málaga
Adra
Almería
BF
CD
ALME
CG
MALA
Arc
Alboran Sea
EAB
AC
YF
Alboran Is
WAB
AF
AR
Figs. 3,4 and 5c
Mw 6.3
SAB
MELI
Melilla
NF
Gibraltar
Rif
Al Hoceima
TF
a
b
c
N
37°
36°
2°
South-Iberian & Maghrebian cover
Alboran Domain
Mud-diapir province
Volcanic rocks
Faults
African foreland
Neogene basins
Flysch trough units
Syncline
Anticline
Seismicity Mw>3 (1990-2017)
GPS motion
New data
5 mm/yr
Palano et al. (2015)

Fig. 2.

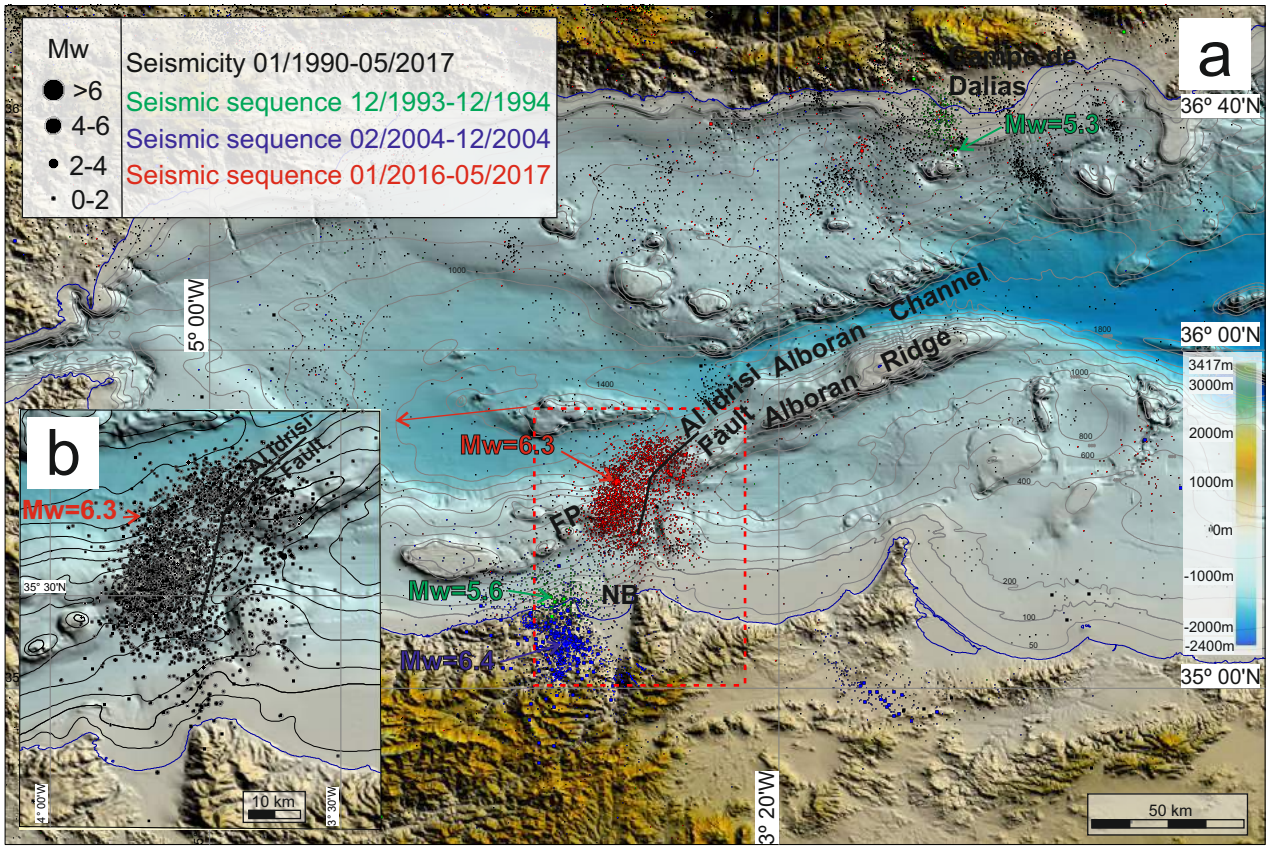
Mw
>6
4-6
2-4
0-2
Seismicity 01/1990-05/2017
Seismic sequence 12/1993-12/1994
Seismic sequence 02/2004-12/2004
Seismic sequence 01/2016-05/2017
a
b
Dalias
Mw=5.3
36° 40'N
36° 00'N
35° 00'N
5° 00'W
3° 20'W
Alboran Channel
Alboran Ridge
Al Idrisi Fault
Mw=6.3
FP
Mw=5.6
NB
Mw=6.4
3417m
3000m
2000m
1000m
0m
-1000m
-2000m
-2400m
50 km
10 km
35° 30'N
4° 00'W
3° 30'W

Fig. 3.

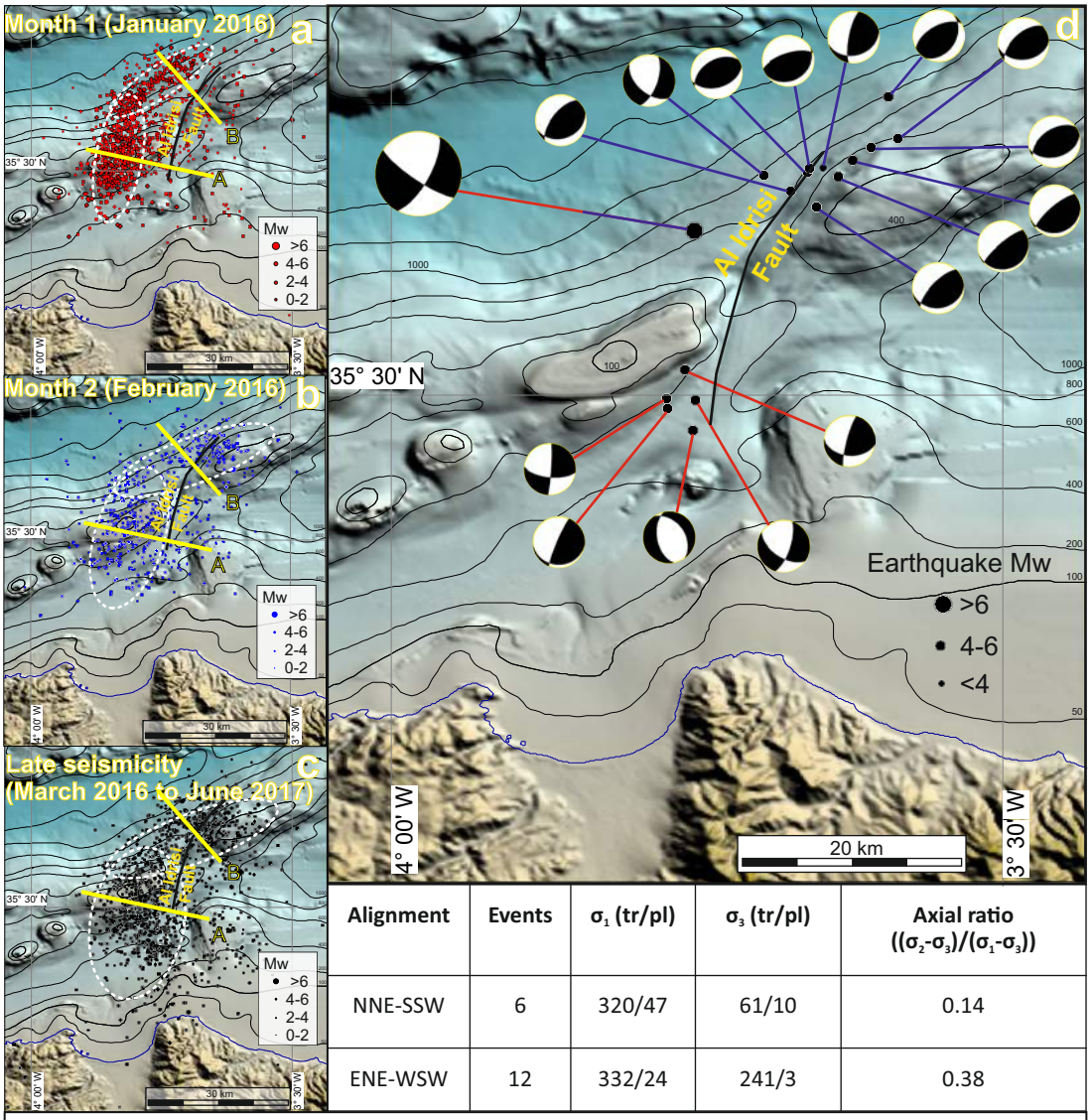

Alignment	Events	σ_1 (tr/pl)	σ_3 (tr/pl)	Axial ratio $((\sigma_2-\sigma_3)/(\sigma_1-\sigma_3))$
NNE-SSW	6	320/47	61/10	0.14
ENE-WSW	12	332/24	241/3	0.38

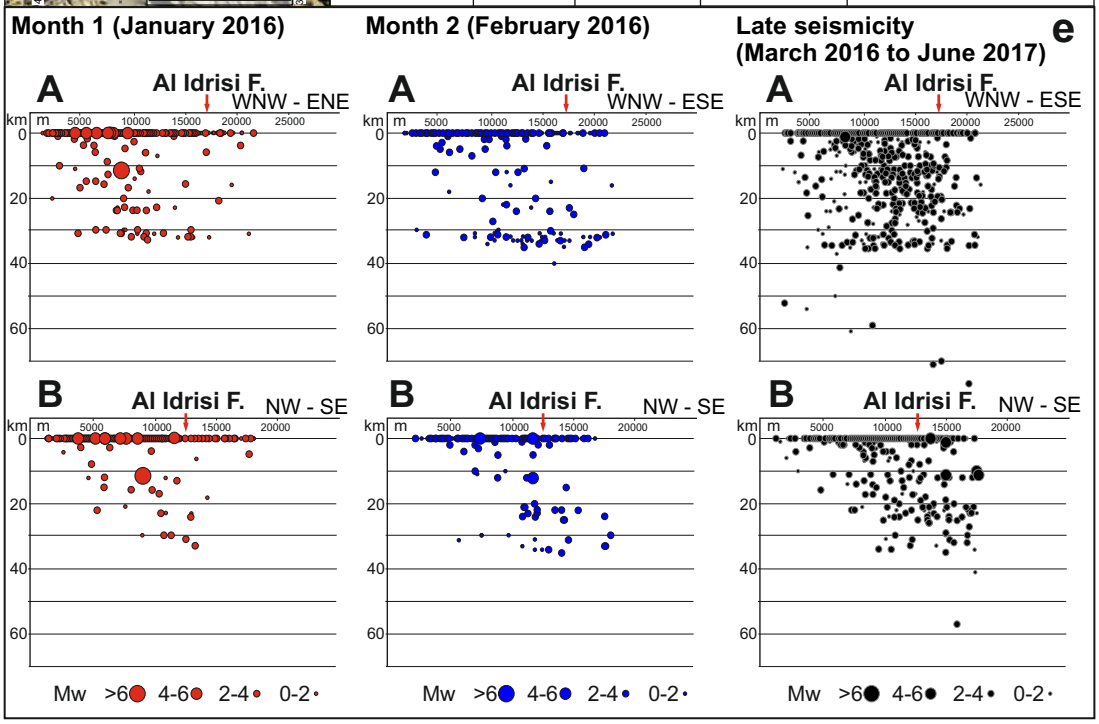

Fig. 4.

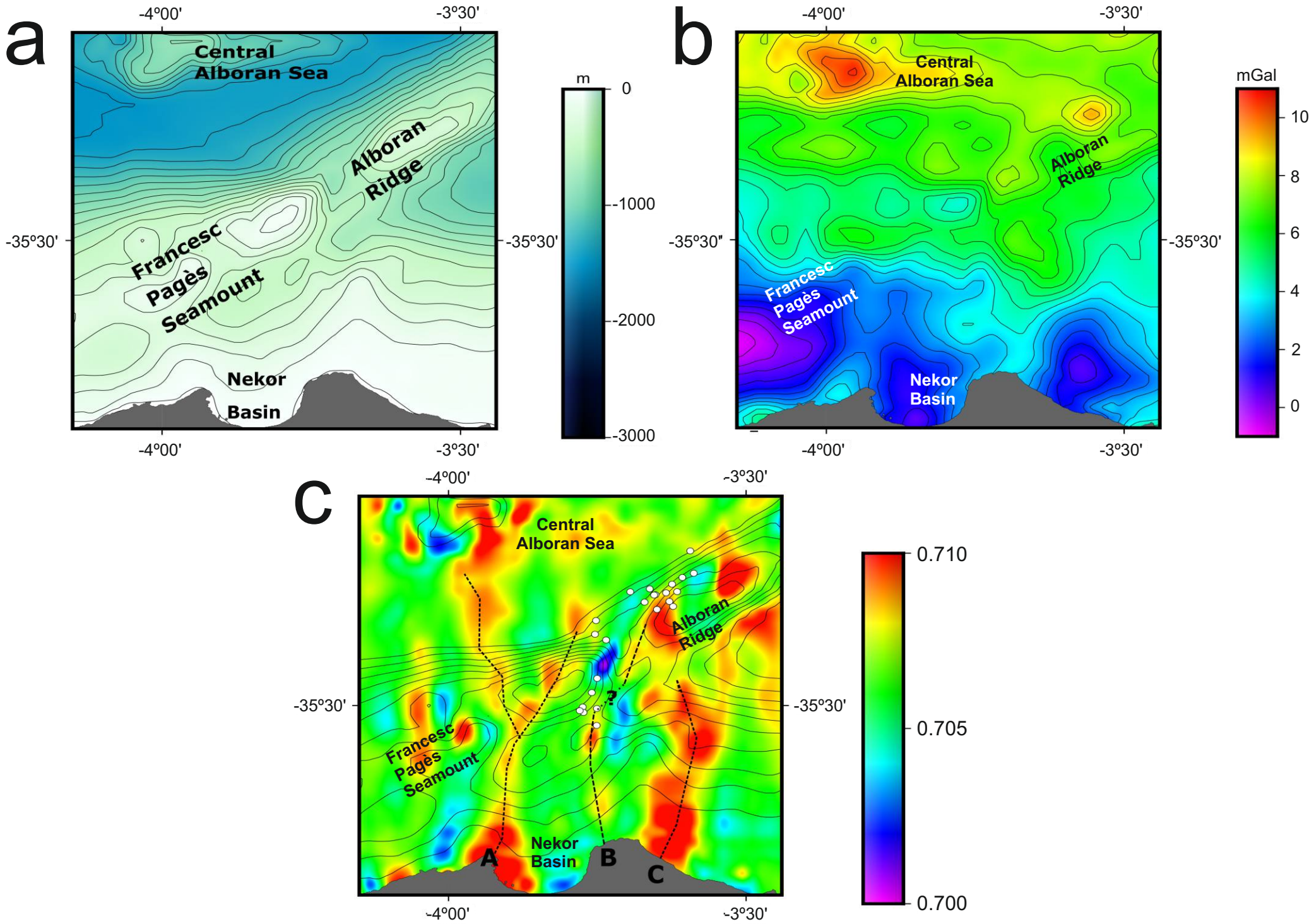
a
-4°00'
-3°30'
-35°30'
Central
Alboran Sea
Alboran
Ridge
Francesc
Pagès
Seamount
Nekor
Basin
m
0
-1000
-2000
-3000
b
mGal
10
8
6
4
2
0
C
A
B
C
?
0.710
0.705
0.700

Fig. 5.

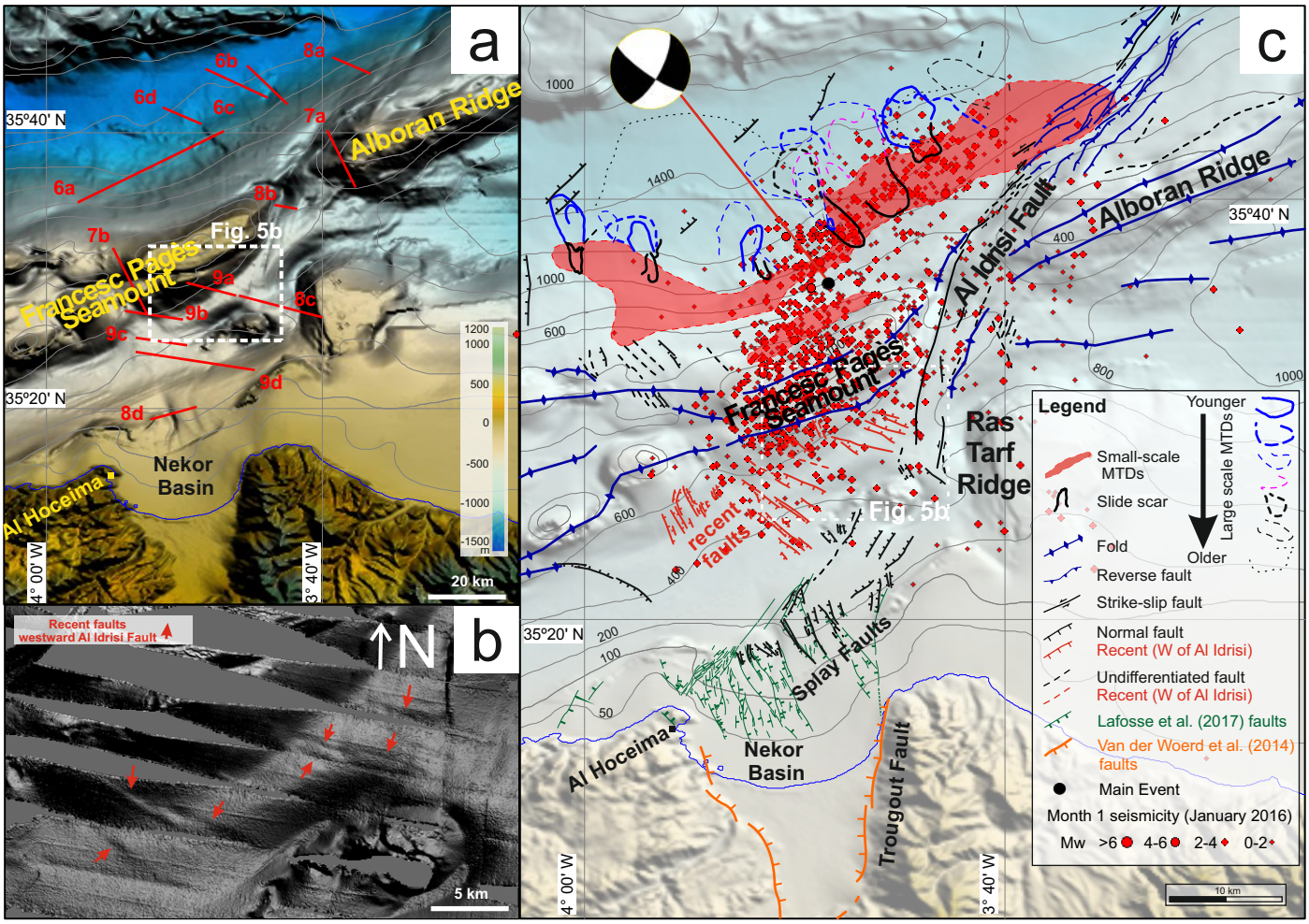
a
b
c
Alboran Ridge
Fig. 5b
Francesc Pages Seamount
Nekor Basin
Al Hoceima
35°40' N
35°20' N
4° 00' W
3° 40' W
20 km
5 km
Recent faults westward Al Idrisi Fault
↑N
Al Idrisi Fault
Ras Tarf Ridge
recent faults
Splay Faults
Trougout Fault
Legend
Younger
Older
Large scale MTDs
Small-scale MTDs
Slide scar
Fold
Reverse fault
Strike-slip fault
Normal fault
Recent (W of Al Idrisi)
Undifferentiated fault
Recent (W of Al Idrisi)
Lafosse et al. (2017) faults
Van der Woerd et al. (2014) faults
Main Event
Month 1 seismicity (January 2016)
Mw >6 4-6 2-4 0-2
10 km

Fig. 6.

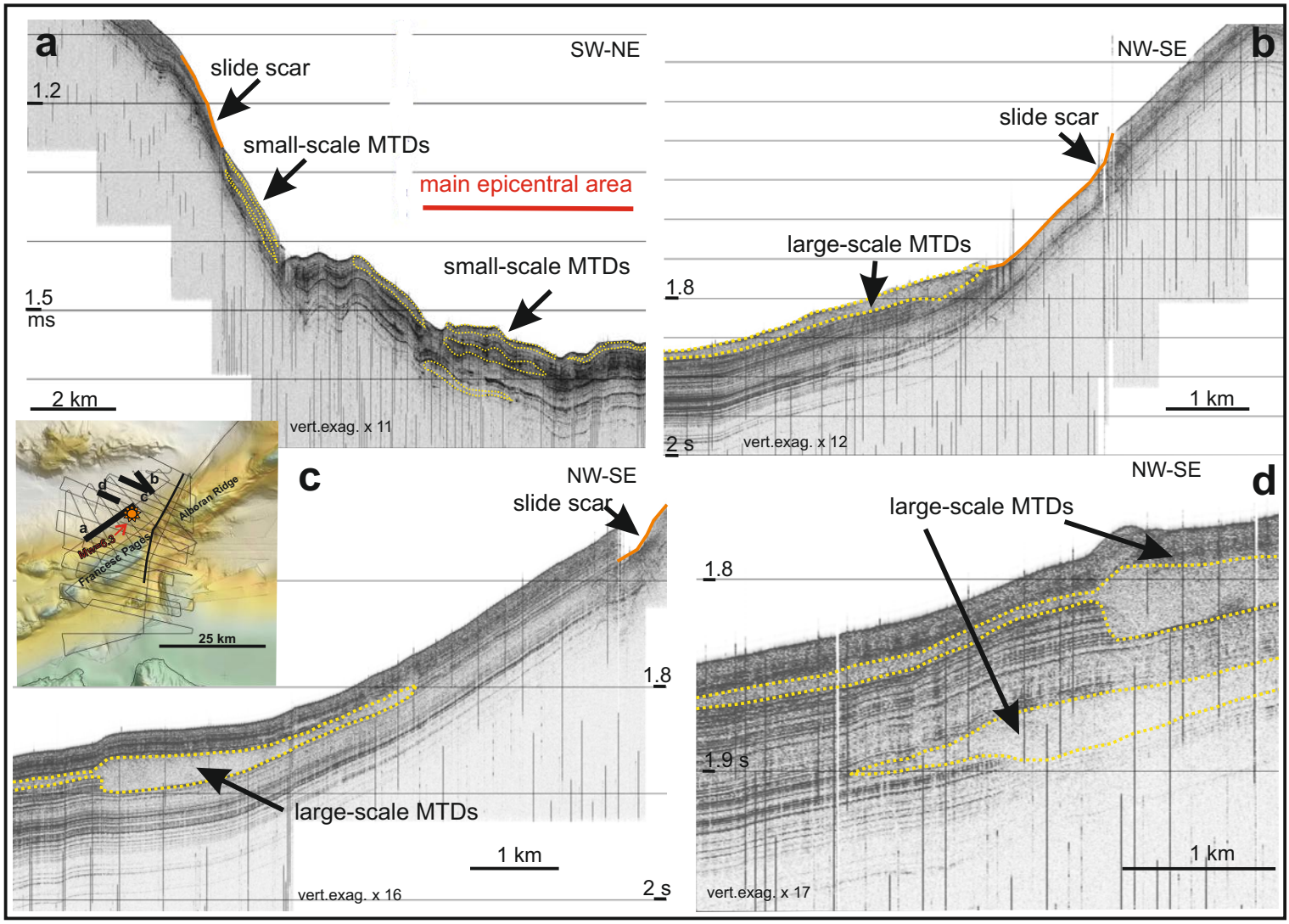
a
SW-NE
slide scar
1.2
small-scale MTDs
main epicentral area
small-scale MTDs
1.5
ms
2 km
vert.exag. x 11
b
NW-SE
slide scar
large-scale MTDs
1.8
1 km
2 s
vert.exag. x 12
c
NW-SE
slide scar
1.8
large-scale MTDs
1 km
2 s
vert.exag. x 16
d
NW-SE
large-scale MTDs
1.8
1.9 s
1 km
vert.exag. x 17
a
b
c
Alboran Ridge
Mw=6.3
Francesc Pagès
25 km

Fig. 7.

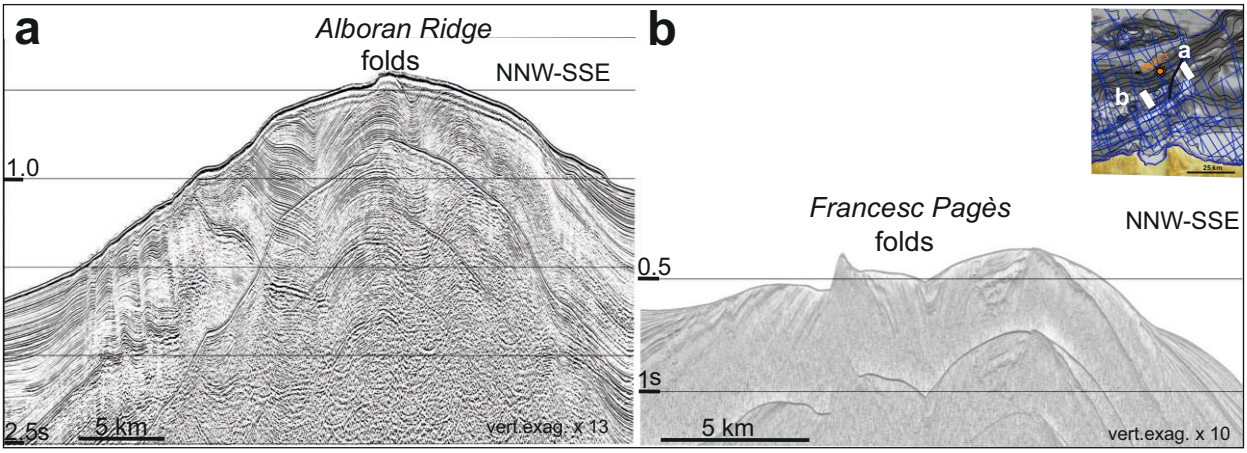
a
Alboran Ridge
folds
NNW-SSE
1.0
2.5s
5 km
vert.exag. x 13
b
a
b
25 km
Francesc Pagès
folds
NNW-SSE
0.5
1s
5 km
vert.exag. x 10

Fig. 8.

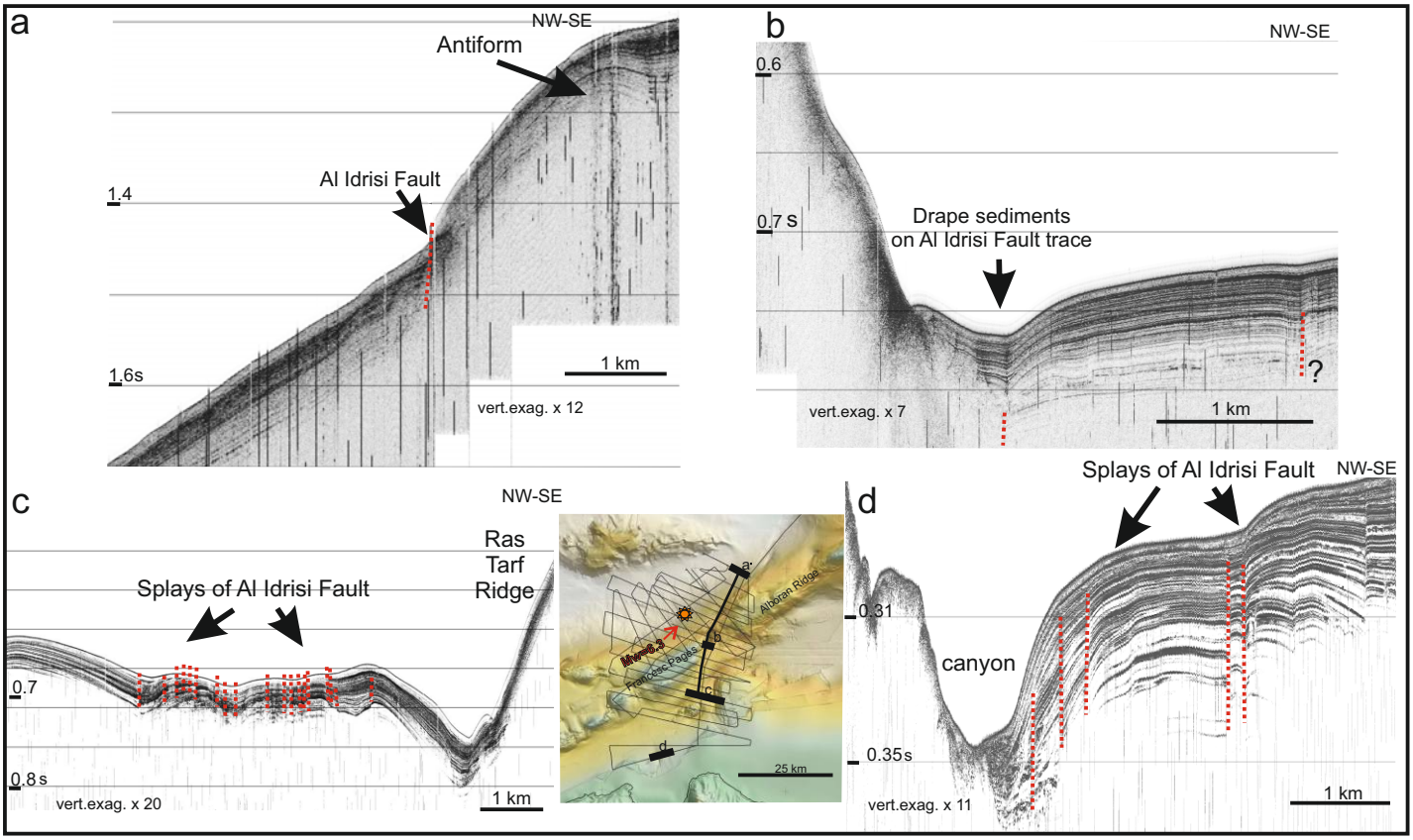
a
NW-SE
Antiform
Al Idrisi Fault
1.4
1.6s
1 km
vert.exag. x 12
b
NW-SE
0.6
0.7 s
Drape sediments
on Al Idrisi Fault trace
?
vert.exag. x 7
1 km
c
NW-SE
Ras
Tarf
Ridge
Splays of Al Idrisi Fault
0.7
0.8 s
vert.exag. x 20
1 km
Alboran Ridge
Mw6.3
Francisco Pacheco
a
b
c
d
25 km
d
Splays of Al Idrisi Fault
NW-SE
0.31
canyon
0.35s
vert.exag. x 11
1 km

Fig. 9.

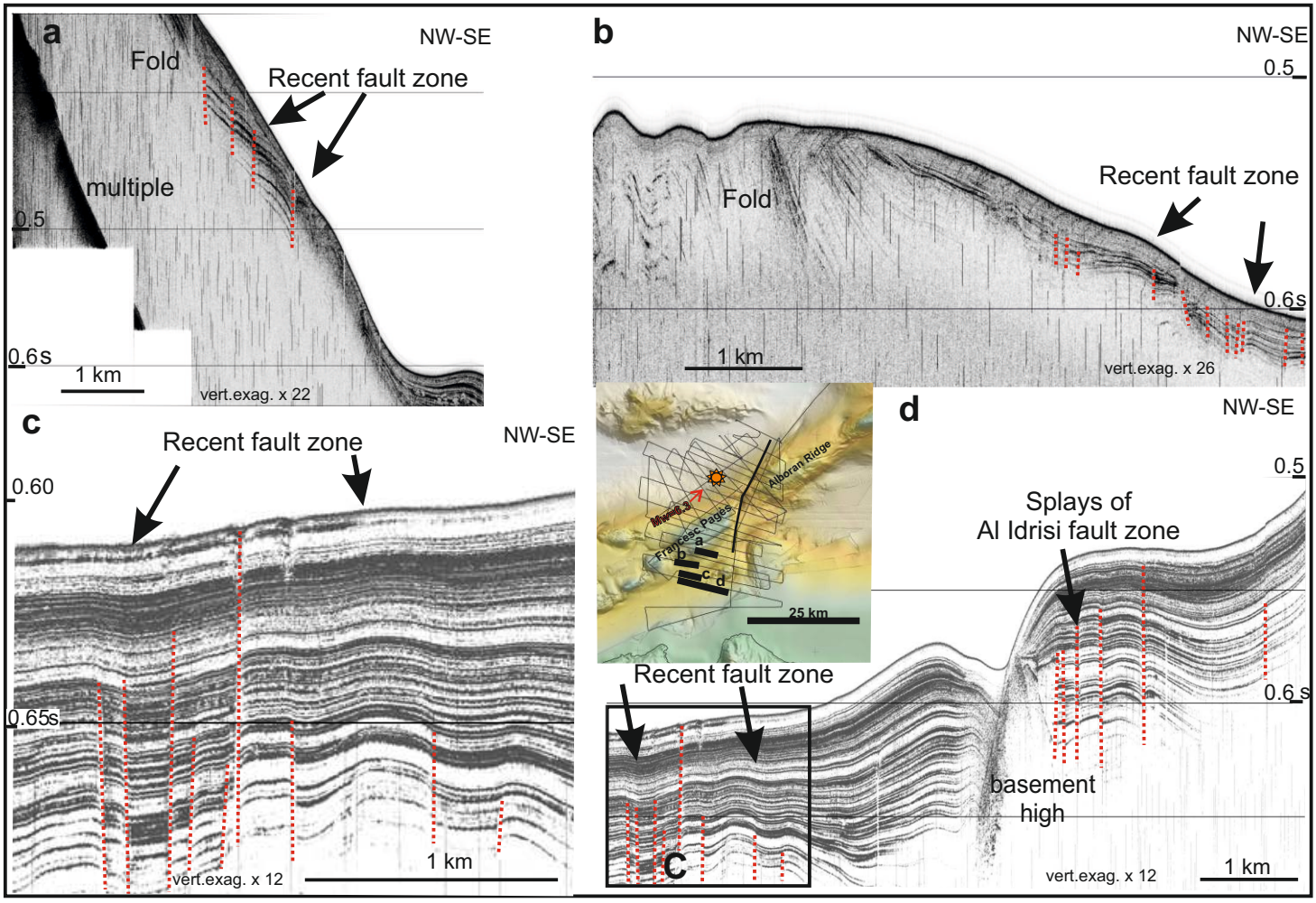
a
NW-SE
Fold
Recent fault zone
multiple
0.5
0.6s
1 km
vert.exag. x 22
b
NW-SE
0.5
Fold
Recent fault zone
0.6s
1 km
vert.exag. x 26
c
Recent fault zone
NW-SE
0.60
0.65s
vert.exag. x 12
1 km
Alboran Ridge
Francesc Pages
a
b
c
d
25 km
d
NW-SE
0.5
Splays of
Al Idrisi fault zone
Recent fault zone
0.6s
basement
high
C
vert.exag. x 12
1 km

Fig. 10.

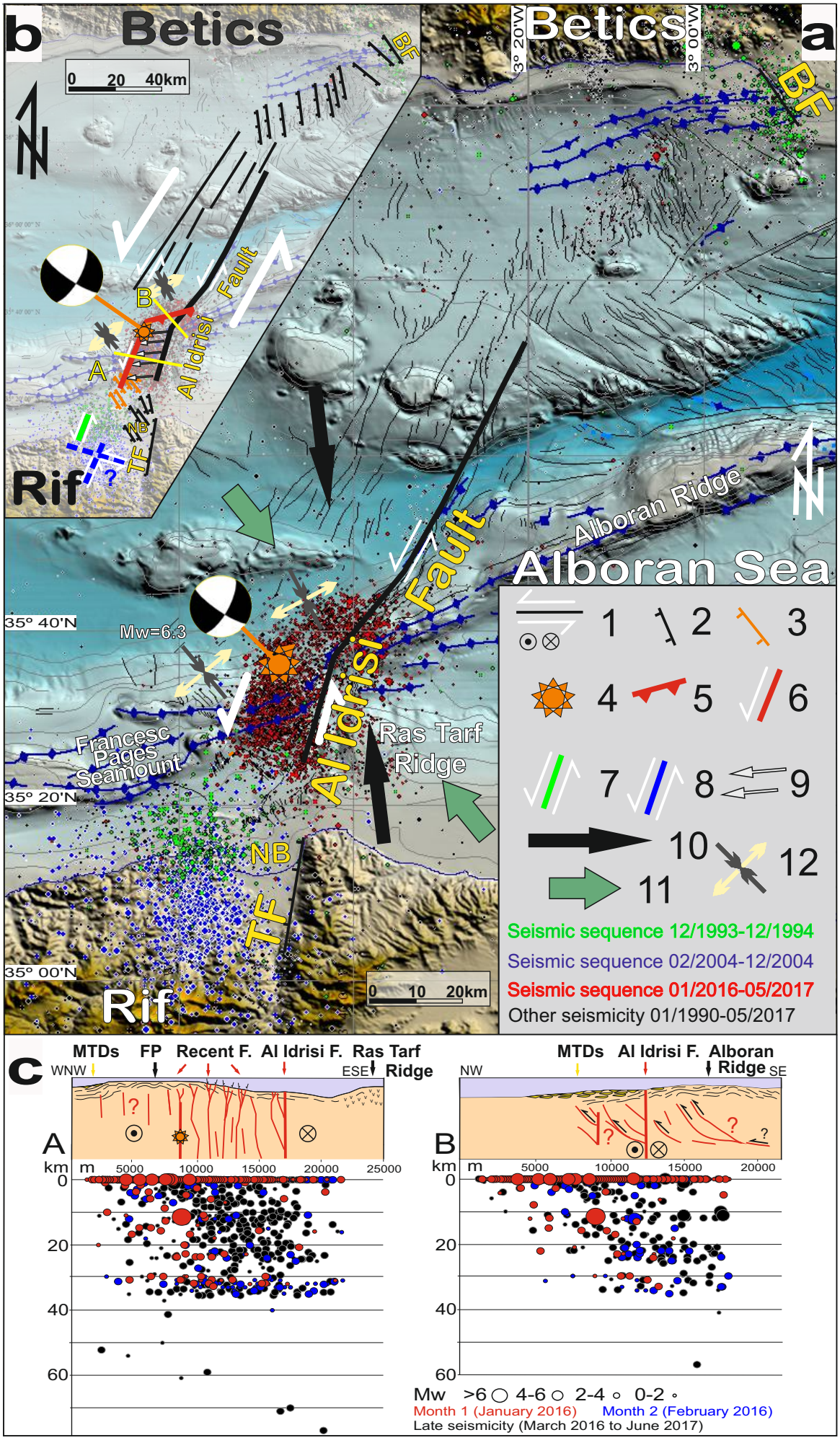
b
Betics
0 20 40km
BF
Al Idrisi Fault
B
A
NB
TF
Rif
?
a
Betics
3° 20'W
3° 00'W
BF
Alboran Ridge
Alboran Sea
Al Idrisi Fault
35° 40'N
Mw=6.3
Francesc Pages Seamount
35° 20'N
Ras Tarf Ridge
NB
TF
35° 00'N
Rif
0 10 20km
1 2 3
4 5 6
7 8 9
10 12
11
Seismic sequence 12/1993-12/1994
Seismic sequence 02/2004-12/2004
Seismic sequence 01/2016-05/2017
Other seismicity 01/1990-05/2017
c
MTDs FP Recent F. Al Idrisi F. Ras Tarf Ridge
WNW ESE
A
km m 5000 10000 15000 20000 25000
0 20 40 60
MTDs Al Idrisi F. Alboran Ridge
NW SE
B
km m 5000 10000 15000 20000
0 20 40 60
Mw >6 ◯ 4-6 ○ 2-4 ∘ 0-2 ∘
Month 1 (January 2016) Month 2 (February 2016)
Late seismicity (March 2016 to June 2017)